A MATHEMATICAL MODELING STUDY ON THE INTENSIFICATION OF THE WATER-GAS SHIFT REACTION

by

Orhun Harmancılar

B.S., Chemical Engineering, Bogazici University, 2022

Submitted to the Institute for Graduate Studies in
Science and Engineering in partial fulfillment of
the requirements for the degree of
Master of Science

Graduate Program in Chemical Engineering

Boğaziçi University

2024

ACKNOWLEDGEMENTS

First and foremost, I would like to extend my biggest gratitude to my research advisor Prof. Dr. Ahmet Kerim Avcı, whose guidance, support, and expertise were invaluable not only in this research journey but throughout my whole undergraduate and graduate period of study. His dedication to excellence, his insightful feedback, his vision and deep knowledge significantly contributed to the completion of this work and allowed me to expand my own knowledge.

I am also thankful to and Prof. Ramazan Yıldırım and Prof. Ayşe Nilgün Akın for generously dedicating their time to review and evaluate my research.

Special thanks to Hasan Köybaşı for who has been a great mentor throughout this research journey. His very informative teachings and feedbacks especially in the areas of modelling was the cornerstone for the completion of my both graduate and graduate research. I am also very thankful to my old and new laboratory co-members, Mert Can İnce, Mert Özden, Semih Altınsoy, Emre Küçük, Damla Sıvacı, İrem Taşpınar, and Gözde Kara, whose collaboration, support, academic help but maybe the most importantly, their friendship made the research environment stimulating and enjoyable. Their collective effort and willingness to share knowledge were instrumental in overcoming challenges and achieving our research goals.

To my family, I owe an immense debt of gratitude. My father, Murat Harmancılar, is always my biggest supporter, helper, motivator and the first person that I take as an example for myself both as a person and an engineer. Taking his engineer side as an example, he has instilled in me a passion for precision and a relentless pursuit of excellence in my academic endeavors.

I am equally thankful for my brother, whose unwavering support and positive influence have been a constant in my life. His encouragement and belief in my abilities have motivated me to push beyond my limits and strive for success in every endeavor.

I also extend heartfelt thanks to my mother, Ayten Harmancılar, for her unconditional love and unwavering support. Her nurturing presence has provided me with strength and encouragement throughout my academic journey.

Lastly, I would like to thank all those who supported me in various ways during this research endeavor. Your encouragement and assistance have been deeply appreciated.

Financial support is provided by Bogazici University Research Fund Grant number 19923.

ABSTRACT

A MATHEMATICAL MODELING STUDY ON THE INTENSIFICATION OF THE WATER-GAS SHIFT REACTION

Low temperature water gas shift (WGS) reaction is modeled over a $CuO/ZnO/Al_2O_3$ catalyst in the presence of a ZIF-7 membrane. Upon validation of the model with the literature-based experimental data, effects of the flow arrangement, sweep gas type and flow rate, pressure and gas hourly space velocity (GHSV) on CO conversion are analyzed and permeated H_2 flow rate is determined at different pressures. During the parameter analysis, performance of ZIF-7 membrane is also compared with a Pd-Ag membrane under the same reaction conditions. Ultimately, it is found that the best performance corresponding to 98% CO conversion is observed at 800 h^{-1} GHSV, and 10 bar with 1.072 $mol.h^{-1}$ co-current steam flow used as the sweep gas. Employing steam as the sweep gas resulted in significant CO conversion improvement and co-current arrangement is found to be essential for keeping the temperature profile isothermal. Moreover, ZIF-7 shown significantly better performance than Pd-Ag membrane due to the reverse permeation of steam in ZIF-7 reactor. Low temperature WGS reaction model is followed by a ZIF-7 membrane microreactor model that involved $Pt\text{-}CeO_2$ catalyst. After the validation of reactor model and kinetics, similar parameter analysis also performed for ZIF-7 membrane microreactor. Effects of sweep type and molar flow rate, pressure and residence time are investigated. Also, the same model is run in a mode that reflects the conventional two adiabatic consecutive reactors that operates over Fe/Cr (First reactor) and $CuO/ZnO/Al_2O_3$ (Second reactor), and the data gathered are compared with the single reactor $Pt\text{-}CeO_2$ data. Parameter analysis shown that at 10 bar, using steam as the sweep gas at 10 times of the retentate inlet flow rate in co–current flow is the most beneficial and 100% conversion can be achieved as the residence time is increased to 35.55 g.h/mol. Moreover, comparison studies shown that single unit membrane reactor with 11.85 g.h/mol residence time at 400°C result in a superior performance (94.54% CO conversion) compared to the conventional reactor model.

ÖZET

SU GAZI DEĞİŞİMİ TEPKİMESİNİN YOĞUNLAŞTIRILMASINA YÖNELİK BİR MATEMATİKSEL MODELLEME ÇALIŞMASI

Düşük sıcaklık su gazı değişimi (SGD) reaksiyonu $CuO/ZnO/Al_2O_3$ katalizörü ve ZIF-7 membranı kullanılan bir reaktörde modellenmiştir. Modelin literatür bazlı deneysel veriler ile teyit edilmesini takiben, süpürücü gaz türünün ve akış hızının, basıncın ve boşluk hızının CO dönüşümü üzerine olan etkileri incelenmiş ve farklı basınçlarda ayrıştırılan H_2'nin akış hızı belirlenmiştir. Ek olarak bu parametrelerin analizi sırasında, ZIF-7 membranının performansı aynı koşullarda yaygınca kullanılan Pd-Ag membranıyla karşılaştırılmıştır. Sonuç olarak, %98 CO dönüşümüyle en iyi performansın 800 h^{-1} ve 10 bar'da; 1.072 $mol.h^{-1}$ süpürücü su buharının eşyönlü akışı sırasında gerçekleştiği saptanmıştır. Özellikle süpürücü gaz olarak su buharının kullanılmasının CO dönüşümüne büyük katkı sağladığı ve eşyönlü akışın sıcaklık profilini sabit tutmak için kritik bir faktör olduğu bulunmuştur. Bunun yanında, ZIF-7 membranının su buharının membrandan ters geçişi sayesinde Pd-Ag membranından çok daha iyi performans gösterdiği gözlemlenmiştir. Bu çalışmanın devamında katalizör olarak Pt-CeO_2'nin ve membran olarak ZIF-7'nin kullanıldığı bir membran mikroreaktörü modellenmiştir. Reaktör modelinin ve reaksiyon kinetiğinin onaylanması sonucunda ilk modele benzer bir parametre analizi gerçekleştirilmiştir. Burada süpürücü gazın türünün ve akış hızının, basıncın ve akışın kanalda kalma süresinin etkileri araştırılmıştır. Ek olarak, aynı model geleneksel, ardışık adiyabatik modda çalıştırılan ve ilki Fe-Cr, ikincisi $CuO/ZnO/Al_2O_3$ katalizörü içeren iki reaktörü modellemek için kullanılmış ve elde edilen veri önceki tek reaktör sistemiyle karşılaştırılmıştır. Sonuçlara göre 10 bar basınç, reaksiyon kanal girişi akış hızının 10 katı kadar eşyönlü süpürücü su buharı en iyi performansı göstermiştir. Kanalda kalış süresi 35.55 g.h/mol'e yaklaştığında %100 dönüşümün sağlanabileceği görülmüştür. Ayrıca tek ünite Pt-CeO_2 membran mikroreaktörünün 400°C'de 11.85 g.h/mol kalış süresiyle %94.54 dönüşüme ulaşıp çift reactor sistemine göre daha üstün olduğu saptanmıştır.

TABLE OF CONTENTS

LIST OF FIGURES

LIST OF TABLES

LIST OF SYMBOLS

a	Reaction Order of CO concentration
b	Reaction Order of CO_2 concentration
C_i	Concentration of species i (kmol m^{-3})
$C_{p,i}$	Heat capacity of species i (J mol^{-1} K^{-1})
c	Reaction Order of H_2 concentration
d	Reaction Order of H_2O concentration
F_i	Molar flow rate of the species i (mol h^{-1})
i	Species
J_i	Permeation flux of component i (mol m^{-2} s^{-1})
K_{eq}	Reaction equilibrium constant
K_i	Adsorption/desorption equilibrium constant for species i (Pa^{-1})
k	Reaction rate constant for reaction (mol g_{cat}^{-1} h^{-1})
P	Pressure (bar)
P_i	Partial pressure of species i (Pa)
Pe_i	Membrane permeability of species i (mol m^{-2} s^{-1} Pa^{-1})
R	Ideal gas constant (8.3144 J mol^{-1} K^{-1})
r	Reaction rate (mol h^{-1} g_{cat}^{-1})
$-r_{CO}$	Rate of consumption of CO (mol h^{-1} g_{cat}^{-1})
S_m	Membrane area per bed volume (m^{-1})
T	Temperature (K)
U	Overall Heat transfer Coefficient (J m^{-2} h^{-1} K^{-1})
V_R	Reactor volume (m^3)
v_i	Reaction stoichiometry of species i
w_{cat}	Catalyst weight (g)
ΔH°_{rxn}	Heat of reaction (kJ mol^{-1})
ρ_b	Bed Density (g m^{-3})

LIST OF ACRONYMS/ABBREVIATIONS

1D	One Dimensional
BET	Brauner-Emmett-Teller
C_3H_8	Propane
CCD	Catalytic Cracking Deposition
CCSU	Carbon Capture Storage and Utilization
CFD	Computational Fluid Dynamics
CH_4	Methane
CO	Carbon Monoxide
CO_2	Carbon Dioxide
DFT	Density Functional Theory
DRIFTS	Diffuse Reflectance Infrared Fourier Transform Spectroscopy
GHSV	Gas Hourly Space Velocity (h^{-1})
H_2	Hydrogen
H_2O	Water
HTC	High Temperature Catalyst
IEA	International Energy Agency
MDES	Methyldiethoxysilane
MFI	Mobil-type Five
MIL	Materials of Institute Lavosier
MOF	Metal Organic Framework
N_2	Nitrogen
NO_x	Nitrogen Oxides
P	Permeate
PBR	Packed Bed Reactor
PEMFC	Proton Exchange Membrane Fuel Cell
PM	Particulate Matter
PSD	Pore Size Distribution
PSS	Porous Stainless Steel
R	Retentate
RIMF	Retentate Inlet Molar Flowrate

SMR	Steam Methane Reforming
SO_x	Sulphur Oxides
STP	Standard Temperature and Pressure
TEM	Transmission Electron Microscopy
TPR	Temperature Programmed Reduction
UHC	Unburned Hydrocarbons
WGS	Water Gas Shift
WHSV	Weight Hourly Space Velocity (h^{-1})
XRD	X-ray Diffraction
ZIF	Zeolite Imidazolate Framework

1. INTRODUCTION

Energy demands continue to grow as the population of earth also continues to increase. Despite the recent advancements cleaner energy production methods such as solar, wind, hydro and nuclear energy, huge attention on the electrification of the processes and utilization of carbon-free energy production methods such as biofuels [1] coal, natural gas and oil are still the world's primary energy resource for the majority of industrial processes. According to World Energy Outlook rapport of International Energy Agency (IEA) at 2023[2], this rise in fossil fuel usage is expected to increase until 2030 and high rate of usage of Natural gas and oil will continue to be present at least until 2050 , as coal usage starts to diminish.

As a result of the long history of fossil fuel usage through combustion, emissions of greenhouses gases and air pollutants such as CO, NO_x, SO_x, PM, and UHCs polluted and will continue to pollute the atmosphere.[3]. In addition to these, another product of these fossil fuel processes, CO_2, is one of the leading reasons of the global warming and climate change since the rise of industrial processes during Industrial Revolution. Since that, carbon capture, storage and utilization processes (CCSU) are crucial to reduce the harmful impact of CO_2. These processes are separated into three group depending on the employed combustion process, namely pre-combustion, post- combustion and oxyfuel combustion.

In oxyfuel combustion, combustion occurs using pure oxygen, resulting in flue gas with a high concentration of CO_2 and capture processes are employed to contain the resultant CO_2. Post combustion involves the capture process employed downstream of the combustion process. Pre - combustion processes involve the partial oxidization of the fuel by oxygen, steam or air to produce syngas and CO_2 capture process, here, takes the shape of a Water Gas Shift (WGS) Reactor that produces an effluent fluid stream with higher H_2 and lower CO concentrations. Additionally, because of the increased concentration of CO_2 and H_2 in the processed gas, capturing and separating CO_2 from the product stream is facilitated [3,4].

Hydrogen also plays a crucial role in shifting the energy sources from fossil fuels to other renewable energy sources. It is one of the most important aspects in non-carbon energy producing methods and even itself can be considered as a non-energy source but it is mostly addressed as a great energy carrier due to its very high energy density. [5,6] Together with the natural gas, they can be solely used in internal combustion engines and even can lead to their replacement with fuel-cell applications.[6]. A version of fuel cells, namely proton exchange membrane fuel cells (PEMFC), requires H_2 to generate electricity for both mobile and stationary application that, scales up to around 2-3 kW and WGS reaction is the primary source of this necessary H_2 and part of the CO capture process which is poisonous for the downstream PEMFC unit.[7,8] Additionally, WGS is also the irreplaceable part of the industry scale processes such as NH_3 Synthesis through Haber Bosch Process and synthesis of hydrocarbons to be used as fuels through Fischer Tropsch Synthesis at the upstream. It usually follows a type of a methane reformer, which most widely takes the version of a steam - methane reformer (SMR). This combination of SMR with WGS reaction is approximately responsible for the production of 80% of the hydrogen being produced in industry [9]. SMR reaction is given as

$$CH_4 + H_2O \leftrightarrow CO + 3H_2 \quad \Delta H^{\circ}_{298} = +206\ \frac{kJ}{mol} \tag{1.1}$$

and accompanying WGS reaction is given as

$$CO + H_2O \leftrightarrow CO_2 + H_2 \quad \Delta H^{\circ}_{rxn,298} = -41\ \frac{kJ}{mol}. \tag{1.2}$$

Conventional WGS reaction necessitates two consecutive reactors since it is a thermodynamically limited process at elevated temperatures due to its thermodynamic nature. In this typical arrangement, first high temperature reactor operates adiabatically at 573-673 K (300 - 400°C) inlet temperature range and comprises Fe-Cr based catalysts. The aim at this stage is to benefit from the faster kinetic rates due to the high temperature values [11,12] and CO conversion is limited due to the thermodynamic barrier. This unit is followed by the low temperature WGS reaction and operates at a temperature range of 473-573 K (200 - 300°C) under a packed Cu-Zn catalyst [11]. At lower temperatures, copper (Cu) exhibits high activity for WGS reaction. However, effectiveness of it starts to decline around 600 K due to the significant risk of hydrothermal sintering beyond 300°C temperature.

Because of this, noble metal catalysts such as Ir, Au and Pt (e.g. Pt-CeO_2) recently become more attractive due to their activity in a broader temperature range and can rule out the necessity of using two reactors rather than one.[13] However, research also shown that Pt-CeO_2 starts to lose its activity at temperatures close to 620 K (347°C) due to the thermodynamic limitation. Therefore, applications that involves the simultaneous removal of H_2 to promote further CO conversion via H_2 permselective membrane is a considered strategy by many scientists.

Among the materials suitable for the membranes that can be used for the removal of H_2, Pd and Pd-Ag membranes are the common choice due to their infinite permselectivity towards H_2. However, despite this high permselectivity, H_2 permeance levels are usually found limited. Additionally, due to its high cost and possibility of H_2S poisoning, [14] various silicas, polymers, zeolites, and other Metal Organic Framework (MOF) materials are investigated for their availability for H_2 separation under thermally challenging conditions. Among these materials, MOF sub-groups such as MILs, UiOs and Zeolite Imidazolate Framework (ZIF) materials are investigated by several researchers. Several variations of ZIF materials such as ZIF-7, ZIF-8, ZIF-22, ZIF-90 and ZIF-95 are found especially promising due to their high thermochemical stabilities and tunability of their pore structures. Despite lacking the infinite selectivity towards H_2, ZIF membranes have relatively higher permeance values compared to Pd membranes and can be prepared at a lower cost. [15]

In the applications with fuel processors, WGS unit is expected to be small and lightweight. However, reaching higher CO conversion is only available at lower temperatures due to thermodynamically limited nature of the reaction at higher temperatures. This requires WGS reaction to occur at lower temperatures where kinetic rates of the reaction is slower, causing a larger volume of a reactor to be used to achieve expected CO conversion. Fast removal of heat from the reaction medium is the usual method to bypass thermodynamic limitation but packed bed reactors having poor heat transfer qualities, microreactor applications are the alternative choices due their high ratio of surface area per volume. Additionally, this high ratio makes microreactors very eligible for membrane application, since membranes can offer a large surface area for mass transfer processes to occur. [16]

In this study, WGS reaction is modelled in two versions that uses ZIF-7 as the membrane material and they are referred based on the employed catalyst in the respective model. In the first model, $Cu/ZnO/Al_2O_3$ (Referred as Cu/Zn for simplicity) catalyst is used to model low temperature WGS reaction and parameters such as flow type, arrangement and rate, pressure and Gas Hourly Space Velocity (GHSV) are analyzed. Same model is also used with a Pd membrane and results are compared with each other. In the second model, $Pt\text{-}CeO_2$ catalyst is used to model WGS reaction in a microreactor and similar parameter analysis is performed. Following that, process is used to compare the model with the conventional two consecutive adiabatic reactor that has also microreactor geometry.

This thesis includes five sections. First section is the introduction part that explains the importance of studied topic and elucidates the intricacies of the WGS reaction. Second section is the detailed literature survey that delves into the articles that explores the aspects of WGS reaction. Third section is the mathematical modeling that elucidates the methods used to prepare the models. Fourth section is the section that results are presented and the reasonings behind the deductions are explained. Fifth and last section is where the important results are highlighted and summarized.

2. LITERATURE SURVEY

2.1. Catalysts

2.1.1. Fe Based Catalysts

Fe based catalysts are the most common catalysts employed in high temperature WGS reactions. Therefore, it is one of the most researched catalyst types for WGS reactions. Below are the key results gathered from literature with both membrane and membraneless applications.

In the work of Khan et al. [17], various metal ions such as Cr, Mn, Co, Ni, Cu, Zn, and Ce were incorporated into the iron oxide lattice, and their suitability for catalyzing the high-temperature water-gas shift reaction was evaluated. The study focuses on determining the transition metal doped catalysts' activity and their crystallography and morphology through various characterization methods such as X-ray diffraction (XRD), pore size distribution (PSD), and transmission electron microscopy (TEM). To prepare the catalysts, Iron nitrates and a dopant metal nitrate were dissolved in separate deionized water batches, then combined and aqueous ammonia. Here, they made sure that nitrate solution concentration was at a value that yields nano-sized grains. Activity tests are performed in a narrow vertical fixed bed ceramic reactor with an inside diameter of 6.37 mm and 0.1 g catalyst weight at a temperature range of 350 - 550°C and atmospheric pressure. Among all the catalysts, Fe-Ce catalyst gave the highest CO conversion (maximum conversion is around 90-95%) at a high steam to CO ratio (7.0) and 550°C. Catalyst was also able to withstand severe conditions present in the reactor.

Following that study, Reddy et al. [18] explores the performance of Fe-Ce catalysts with different doped metals such as Cr, Co, Zr, Hf, and Mo at low steam to CO ratios together with the evaluation of their sulphur tolerance to get an idea about the stability of the catalyst.

Same methods given in Khan et al. [17] are employed to determine the crystallography of each catalyst. Also, the ceramic reactor that activity tests are performed in has the same qualities, geometry and catalyst weight. Pressure is also at atmospheric pressure but temperature range is 400 - 550°C. At steam to carbon ratio of 3.5, Cr and Co doped Fe/Ce catalysts manages to give high CO conversion between 400 and 500°C. Both achieves a conversion around 90% at 500°C. At steam to carbon ratio of 1.5, both Cr and Co doped Fe/Ce catalysts keep their high activity contrary to other doped catalysts. However, Cr doped catalyst gives the highest CO conversion value (~75%) at 500°C and is the only catalyst that manages to achieve equilibrium conversion at 550°C. Also, all catalyst manages to remain unaffected under 400 ppm sulphur presence due to the ceria preventing magnetite from sulfiding.

Furthermore, Devaiah and Smirniotis [19] investigated how varying the concentrations of both Ce and Cr in the Fe-Ce-Cr catalyst affected the high-temperature water-gas reaction. Additionally, they employed XRD and Raman spectroscopy to investigate lattice strain and disorder, respectively to assess influence of atomic ratios present in the catalyst. Activity test is performed under the same conditions with the previously given two studies at 475-500-525°C and steam to CO ration of 1.5 and 3.5. Ce and Cr atomic fractions on the Fe-Ce-Cr catalyst are changed from 10:0.6:1 to 10:1.2:1. and 10:1:0.6 to 10:1:1.2, respectively. 10:1:1 configuration is found to give the highest conversion around 75% at 525°C. They also performed the tests on the stability of the catalyst with respect to time and catalyst managed to perform at the same activity even after 50 hours whereas conventional Fe_2O_3-Cr_2O_3 catalyst encountered a significant drop in its activity. Expectedly, XRD patterns showed that 10:1:1 configuration has the highest lattice strain since it weakens the metal-oxygen bonds, favoring the WGS reaction. Raman spectroscopy results supported these claims since 10:1:1 configuration has the broader Raman curves compared to other configurations.

Kim et al. [20] constructed a membrane reactor that contains an MFI type zeolite disk as membrane and WGS reaction occurs in the presence of a cerium doped ferrite catalyst. Authors evaluated the effect of pressure on the reaction and membrane's stability to H_2S. Constructed horizontal reactor includes 200 mg catalyst that is spread over the membrane.

Also, the catalyst is pressed from above by a carbon cloth sheet with quartz wool on top. Temperature range is selected as 400-550°C and N_2 gas at atmospheric pressure is employed in the permeate side as sweep gas.

Table 2.1. Reactor parameters and flow conditions for the WGS reaction.

Weight Hourly Space Velocity (WHSV) (h^{-1})	7500 - 60000
Reaction Pressure (atm)	2 - 6
Catalyst Packing Density (g/cm^3)	2.0
N_2 sweep Flow Rate (cm^3/min) (STP)	0 - 40
Steam to CO ratio	1.0 - 3.5
Inlet Fractions	33.3% CO, 25.0% CO_2, 25.0% H_2, 16.7% H_2O

Permeance and selectivity of the membrane varies depending on the mixture and operation time. After 1800 hour WGS operation, permeance of H_2 and H_2/CO selectivity increases from 0.83 to $1.03x10^{-7}$ mol/(m^2.s.Pa) and 12.6 to 14.5, respectively as temperature increases from 400°C to 550°C Thanks to the membrane, CO conversion manages to pass the equilibrium conversions and reaches up to 98% at 550°C and 6 atm.

Chen et al. [21] developed a CFD simulation to discover the intricacies of the high temperature WGS reaction using Fe/Cr catalyst and Pd membrane. They modeled the reaction using commercial software COMSOL Multiphysics 4.0a. Temperature and steam to CO ratio are varied between 400 and 700°C and 1.0 – 3.0, respectively. Also, Pressure is set to 10 atm for retentate side and 1.0 atm for permeate side. Instead of usual inert gasses such as N_2 or Ar, they utilized steam as the permeate gas at 150°C since H_2 can be separated from condensation. Reactor geometry is a two concentric cylinder where the inside cylinder is modeled as the Pd membrane and packed catalyst is modeled between the outer wall and membrane. Permeate and retentate stream is arranged in counter current arrangement. Reactor has 9 and 50 mm of inside and outside diameter, respectively and packed length of the is 150 mm.

Table 2.2. Reactor conditions and membrane parameters.

Inlet Fractions	34.69% H_2, 47.96% CO, 17.35% CO_2
Mass flow rate (kg s^{-1})	Retentate: $1.3x10^{-4}$ Permeate:$1.02x10^{-5}$
Porosity	0.4
Catalyst Density (kg m^{-3})	2476
H_2 Permeance pre exponential factor ($mol.m^{-2}.s^{-2}.Pa^{-0.5}$)	$1.69x10^{-2}$
Activation Energy ($kj.mol^{-1}$)	12.2

Permeance of H_2 is calculated by an Arrhenius type equation in the work of Chen et al. utilizing the given H_2 permeance pre-exponential factor and activation energy in Table 2.2. Then, permeation fluxes are calculated using Sievert's Law.

CO conversion is increased beyond the equilibrium conversion thanks to the usage of the membrane. At maximum, CO conversion approaches 85% conversion at 550°C and steam to CO ratio of 3.0 but starts to decline with increasing temperature. Despite the increase in the permeance of Pd membrane with increasing temperature, thermodynamic limitations causing lower equilibrium conversion starts to offset the effect of the former. Authors also investigated the hydrogen recovery in the permeate side and found that it declines with increasing steam to CO ratio, due to the lower H_2 partial pressure on the retentate channel at a higher steam to CO ratio, leading to a decrease in H_2 permeation. To get an idea about the fact that whether increasing steam to CO ratio is beneficial for the system in terms of obtained H_2 amount at permeate since CO conversion and H_2 recovery are directly and inversely proportional with increasing steam to CO ratio, respectively and reaction stoichiometry is one to one, authors define a parameter that is named as pure H_2 index which is the percent multiplication of the two quantities. These multiplication results show that increasing steam to CO ratio also increases pure H_2 index, thereby suggesting that elevation in CO conversion is sufficient to offset the effect of declining H_2 recovery within the reactor.

2.1.2. Pt Based Catalysts

An excellent initial reference to analyze a comparative study on Pt catalysts supported by various single and composite oxides is the research conducted by Panagiotopoulou and Kondarides [22]. The authors investigated the activity of various Pt catalysts where Pt is dispersed on diverse range of single metal oxides and composite MOx/Al_2O_3 and MOx/TiO_2 supports where M is the metals Ti, V, Cr, Mn, Fe, Co, Ni, Cu, Y, Zr, La, Ce, Nd, Sm, Eu, Gd, Ho, Er and Tm. They performed their activity tests at the temperature range of 150-500°C, with an inlet stream composed of 3% CO, 10% H_2O and balance He, and catalyst weight of 100 mg. They also kept the utilized Pt weight constant by employing 0.5 wt% Pt at every catalyst for kinetic measurements. Among single metal oxides, activity tests shown that Pt/TiO_2 is able to show activity even at lower temperatures (150-300°C). While MgO and SiO_2 supports are found non-active at this temperature range, Co_3O_4 achieves the equilibrium conversion (>95%) at the lowest temperature (350°C) among the single metal oxides. Activity tests performed on $Pt/MO_x/Al_2O_3$ has shown that addition of MO_x makes the catalysis more active at lower temperatures, except Mn. CO conversion on the best catalyst, CoO_x is able to reach equilibrium conversion at 330°C, 20°C lower than that of the Pt/ Co_3O_4. However, Ce doped catalyst is the most active catalyst at lower than 275°C (>20% conversion). Among the $Pt/MO_x/TiO_2$, Ce doped version has the highest activity at lower temperatures (~40% conversion at 250°C). Also, $Pt/MO_x/TiO_2$ catalysts manages to achieve higher conversions than $Pt/MO_x/Al_2O_3$ at every studied temperature.

Following these studies, authors also tested the couple of promising catalysts under more realistic WGS reaction conditions. When they utilized a stream that consist of 3% CO, 10% H_2O, 20% H_2, 6% CO_2 and balance He, $Pt/CeO_x/TiO_2$ gave the highest conversion (~40%) at 375°C. Also, even though having poorer support, $Pt/CeO_x/Al_2O_3$ gave the third best performance after $Pt/NdO_x/TiO_2$. Additionally, despite previously having the couple of most optimal results, it is found that CoO_x- and NiO_x- containing catalysts resulted in the methanation reaction at the presence of CO_2 and H_2, making them unsuitable for realistic WGS operation.

Jeong et al. [23] investigates the possibility of a compact single unit application of a WGS reaction with Pt/CeO_2, Pt/ZrO_2, and $Pt/Ce_{(1-x)}Zr_{(x)}O_2$ catalysts ($Ce_{0.8}Zr_{0.2}O_2$, $Ce_{0.6}Zr_{0.4}O_2$, $Ce_{0.4}Zr_{0.6}O_2$, and $Ce_{0.2}Zr_{0.8}O_2$) and trying to determine the catalytic activity of each support various characterization methods such as BET analysis, X-ray diffraction, CO chemisorption and TPR analysis. BET analysis shows that surface area of the catalyst increases with each small insertion of Zr content on the catalysis. From X-ray diffraction patterns, it is deduced that present crystallography in $Pt/Ce_{0.8}Zr_{0.2}O_2$ and $Pt/Ce_{0.6}Zr_{0.4}O_2$ catalysts includes cubic phases while tetragonal phase is dominant in $Pt/Ce_{0.6}Zr_{0.4}O_2$ $Pt/Ce_{0.4}Zr_{0.6}O_2$ and $Pt/Ce_{0.2}Zr_{0.8}O_2$ catalysts. CO chemisorption indicates that Pt dispersion is highest at $Pt/Ce_{0.8}Zr_{0.2}O_2$ with 66.9% and lowest at $PtCeO_2$ with 37.6%. TPR analysis shows that $Pt\text{-}CeO_2$ can be reduced at the lowest temperature, making it suitable for a single unit applications due to its higher turnover frequency at lower temperatures. Activity test are performed in a microtubular quartz reactor with 6.4 vol% CO, 7.1 vol% CO_2, 0.7 vol% CH_4, 43.0 vol% H_2, 28.4 vol% H_2O, and 14.4 vol% N_2, an inlet composition that reflects a reformed stream at the end of a fuel processor. Temperature range, pressure and gas hourly space velocity (GHSV) is set to 200-360°C, 1.0 atm and 45,515 h^{-1}, respectively. Test results shown that $Pt\text{-}CeO_2$ catalyst achieve the highest CO conversion (~90%) around 320°C with $Pt/Ce_{0.8}Zr_{0.2}O_2$ closely behind. Authors suggest the fact that cubic phase of $Ce_{(1-x)}Zr_{(x)}O_2$ exhibits a greater ability to facilitate the redox couple between Ce^{4+} and Ce^{3+} compared to the tetragonal phase, as the reason for higher conversions for these two catalysts. Also, they indicate that the introduction of zirconium into ceria above 60% led to zirconia agglomeration on the surface of the ceria-zirconia solid solution due to insufficient mixing.

Cornaglia et al. [24] performed an experimental WGS reaction using a $Pt/La_2O_3 \cdot SiO_2$ catalyst both in a conventional reactor and a membrane reactor that contains a Pd - Ag membrane. Conventional reactor operations are performed to assess the stability and activity of the catalyst. The feed stream contained 9% CO, 9-27% H_2 (Steam to CO ratio varies between 1.0 and 3.0) and balance Ar. Reaction is performed at 673 K, 1.0 bar pressure and 1.2-1.5 $x10^6$ h^{-1} GHSV using 8.0 mg catalyst. At steam to CO ratio of 3.0, CO conversion is found to be around 50% and stayed at this value for 43 hours after two shut down periods where pure Ar is passed through the first reactor at 673 K and second reactor at 298 K.

At the end of 155 h following two additional shutdown and lower steam to CO processes, CO conversion still managed to reach 50% conversion.

Membrane reactor is used for both permeability and activity tests. Permeability tests are performed by sending pure H_2 to the reactor and at temperature range of 350-450°C and 1 bar using N_2 as sweep gas with 500 $Nml.min^{-1}$. At the end of the these tests, they observed the infinite selectivity of the membrane and found the Arrhenius type equation that can be used to calculate the H_2 permeability with 5100 J/mol activation energy and 3.46×10^{-8} mol $m^{-1}.s^{-1}.Pa^{-0.5}$ permeability pre-exponential factor. At the activity tests, steam to CO ratio is kept constant at 2 and effect of pressure, sweep gas flow rate and space velocity is investigated. At 723 K, 800 kPa 6240 h^{-1} GHSV, hydrogen recovery CO conversion and H_2 production is found as 80%, 92% and 1.18 $Nm^3\ h^{-1}\ m^{-2}$.

2.1.3. Cu based Catalysts

Dae et al. [25] investigated the activity and selectivity of Cu metal on different catalyst supports such as CeO_2, ZrO_2, MgO and Al_2O_3. Catalyst activity is evaluated between 200-400°C at atmospheric pressure, in a fixed microtubular reactor with 48 mg catalyst (20% Cu loading). GHSV was 36201 h^{-1} and inlet fractions were 6.5vol% CO, 7.1vol% CO_2, 0.7vol% CH_4, 42.4vol% H_2, 28.7vol% H_2O, and 14.5vol% N_2. Between 320 and 400°C, Cu/CeO_2 gave the highest activity, being the only catalyst that managed to achieve equilibrium conversion (~70%) at 400°C. However, it is also the least active catalyst lower than 240°C. Between 200 and 280°C, Cu/ZrO_2 gave the highest conversion reaching 35% conversion at 280°C. They also compared two $Cu\text{-}CeO_2$ catalysts that are differentiated by their preparation method, namely co-precipitated and impregnated $Cu\text{-}CeO_2$ catalysts. Co-precipitated conversion resulted in much higher conversion at lower than 320°C (~20% maximum conversion difference at 240°C), but resulted in a slightly less conversion between 320 and 400°C (~5% maximum conversion difference at 360°C). Lastly stability tests that are performed at 320°C shown that co-precipitated $Cu\text{-}CeO_2$ is able to keep its activity for at least 20 h.

Shim et al. [26] investigated the effect of aging time and temperature on various Cu-Zn-Al catalysts (65:25:10 weight fractions, respectively.) that are prepared by the co-precipitation method and named according to the temperature that they aged at. C20C, C40C, C60C, C80C, and C90C catalysts are the names given for catalysts that are left to age at 20, 40, 60, 80 and 90°C during preparation, respectively. Authors utilized characterization methods such as XRD, BET analysis and H_2-TPR. XRD analysis shown that aging temperature had not any impact on phase composition since XRD patterns were similar and featured the peaks related to the CuO and ZnO crystallites. However, BET surface area of each catalyst were different from each other (C80C having the highest), showing that aging temperature has affected the catalysts physically. Additionally, H_2-TPR results illustrated the expected two peaks that corresponds to the reduction of Cu^{+2} to Cu^{+1} and Cu^{+1} to Cu^0 for all catalysts except C90C, which shown only one broad peak that corresponds to bulk CuO particles. Consequently, authors arrived to the conclusion that aging temperature alters the physicochemical properties of catalysts and C90C is less likely to give high activity compared to the other catalysts. Following activity tests are performed in a fixed bed reactor with $8000h^{-1}$ GHSV and 42.86 vol% H_2, 28.57 vol% H_2O, 14.29 vol% N_2, 7.14 vol% CO_2, 6.43 vol% CO, and 0.71 vol% CH_4 inlet fractions. Temperature range is set to 200 and 240°C. Expectedly, C80C and C90C gave the highest and poorest activity, respectively. C80C managed to reach equilibrium conversion ,95%, at 220°C whereas C90C achieved 85% conversion.

Authors prepared the different versions of C80C catalyst by varying the aging time from 8 to 120 h during preparation and used the same characterization methods to determine their surface structure and activity. XRD patterns also shown no difference for these catalysts and BET analysis resulted in different BET surface area for each catalyst (highest for 120 h version), leading the scientists to the same conclusions they arrived for aging temperature. H_2-TPR results shown that only 72 h and 120 h shown the previously assigned two peaks thereby, expected to give higher activity. Indeed, following activity tests performed under the same conditions resulted in nearly identical curves and highest CO conversions for 72 h and 120 h versions. Both catalysts reached equilibrium conversion at 220°C (~95%). Having no difference in activity and being a shorter duration, optimal aging time is determined as 72 h by the authors despite the slight surface area difference found in BET analysis.

Sagata et al. [27] investigated the Cu catalysts on different metallic supports (AlO_x, FeO_x, ZnO_x, and CeO_x) and used several characterization methods to analyze the interaction between Cu and the metallic support to shed light on the factors that causes the activity of the catalyst to rise. XRD results of each catalysts shown the CuO and the corresponding MO_x peaks except Cu-AlO_x. XPS results that belongs the Cu-ZnO_x and Cu-CeO_x indicated that there are also divalent (Cu_2O) interactions in addition to the monovalent (CuO) interactions for these two catalysts. Activity tests performed at 473 K shown that most active catalysts were Cu-AlO_x and Cu-ZnO_x whereas Cu-CeO_2 was the least active. Also, conversion was the highest for Cu-ZnO_x when its relation with respect to Cu^0 surface area and surface Cu content is investigated.

Li et al. [28] investigated the activity of Cu and Ni containing La-doped cerium oxide Ce(La)O_x catalysts. They performed activity tests at atmospheric pressure with 150 mg catalyst and 100 cm^3/min (8000 h^{-1} GHSV and 80000 h^{-1} GHSV) inlet flow comprising 2% CO, 10.7% H_2O, and balance H_2. Based on the results of 80000 h^{-1} Ni containing catalyst resulted in higher conversions (~95%) above 300°C but fail to keep this high activity at lower temperatures. On the other hand, Cu containing catalyst gives better performance significantly at temperatures lower than 300°C and reaches 90% conversion at 400°C. Authors also performed parameter analysis for GHSV, metal content, H_2 effect on the inlet and steam to CO ratio. Expectedly, 8000 h^{-1} gave much higher conversion compared to 80000 h^{-1} for Cu containing catalyst. Specifically, 90% and 48% conversion are achieved with flows 8000h^{-1} and 80000 h^{-1} at 250°C, respectively. In metal loading tests, Cu loading on Cu-Ce(La)O_2 is varied between 5 and 40% and 20% loading gave the highest conversion due to the formation of bulk CuO at higher loadings. Due to the similar reason Cu-Ce(La)O_2, 5% Ni-Ce(La)O_2 gave the highest conversion among other Ni containing catalysts. When 40% H_2 is added to the inlet instead of a portion of balanced He, Cu conversion reduced significantly above 350°C due to the changed equilibrium conditions. However, lower than 350°C, its effect on CO conversion was negligible. Authors also used an inlet stream with 0.2% CO, 1.5% H_2O and balance He compositions to analyze the effects of different Steam to CO ratios (It is increased from 5.35 to 7.5) with 5% Cu-Ce(La)O_2. Equilibrium conversion (~100%) is reached at 250°C and higher conversions is reached at temperatures lower than 300°C. At maximum, 25% conversion difference is observed at 150°C.

2.2. Membranes

Mendes et al. [29] experimentally investigated the performance of a packed bed membrane reactor with Pd-Ag membrane. Membrane is prepared starting from a commercial 50 μm Pd-Ag metal alloy sheet and shaped into finger like self-supported dense Pd-Ag membrane tubes through annealing and diffusion welding processes. Permeation tests are performed by employing a binary mixture that contains H_2 and N_2 at temperature range of 200-300°C and H_2 permeance is expressed in Arrhenius Equation form. H_2 permeance pre exponential factor and activation energy are found as 5.44 x 10^{-8} mol/(m.s.$Pa^{0.5}$) and 10.72 kj/mol, respectively. Activity tests are performed under 1.5 g $CuO/ZnO/Al_2O_3$ catalyst with an inlet stream comprising 4.70% CO, 34.78% H_2O, 28.70% H_2, 10.16% CO_2 and balance N_2. Temperature range is kept the same and inlet pressure and flowrate of the retentate channel are varied between 1.0 and 4.0 bar and 30 and 270 mL_N min^{-1}, respectively. As a result, the most optimal results (Around 100% conversion and complete recovery of H_2) are gathered at 300°C when GHSV was equal to 1200 L_N $kg_{cat}^{-1}.h^{-1}$, sweep gas flow rate was 1000 mL_N $.min^{-1}$ and Inlet pressure of retentate and permeate channels was 4.0 and 3.0 bar, respectively.

Liguori et al. [30] analyzed the performance of a Pd based membrane supported on a porous stainless steel (Pd/PSS) experimentally under WGS reaction conditions with Fe-Cr catalyst. 20 μm Pd membrane is prepared by electroless plating method on PSS instead of using dense Pd to overcome the issues the dense Pd has such as high cost and low permeance. Authors also claim that choosing PSS instead of other porous materials that are known to be used for such applications such as ceramic, glass or metallic supports reduces the cost and give the membrane higher mechanical strength. Authors analyzed the influence of many parameters on CO conversion such as pressure, GHSV and steam to CO ratio at 390°C. With an inlet stream that comprises 8% CO, 32% H_2O, 24% CO_2, 36% H_2, approximately 80% CO conversion, 70% hydrogen recovery on permeate and around 97% hydrogen permeate purity is achieved at 11 bar and 3450 h^{-1}. Stability of the membrane analyzed by employing several thermal and pressure cycles at 390°C. At the third cycle, H_2 was fed to the membrane module, and the pressure difference across the membrane was kept constant at 1.5 bar.

Membrane managed to offer constant H_2 flux for 1000 h but it dropped 8% by the end of the 1200 h. N_2 and He permeance remained the same during the full time of the experiment. Authors performed the permeation test under both binary (45% H_2, 55% He) mixture and a mixture that contains H_2, CO, CO_2, H_2O with 45%, 8%, 31%, 16% fractions, respectively. Permeating fluxes measured under reaction gases shown reduced results compared to the binary mixture. Specifically, H_2 permeating flux is found to be $4.4x\ 10^{-2}$ $mol/s.m^2$ at 64 $kPa^{0.7}$ partial pressure difference for the binary mixture whereas it is only around $1.2x10^{-2}$ $mol/s.m^2$ at 60 $kPa^{0.7}$ partial pressure difference for the reaction mixture. Authors claims that this reduction occurs due to the competitive adsorption of CO and more prominently, the formation of adsorbed O atoms via H_2O decomposition and recombination mechanism on the Pd surface.

Brunnetti et al. [31] analyzed WGS reaction with a CuO/CeO_2 catalyst and a silica membrane supported on PSS. Silica is advantageous in terms of low cost, thermal stability and high permeation flux but generally gives low permselectivites to H_2. Authors aims to increase this permselectivity via the usage of a mesoporous γ-alumina film. Permeation tests are performed between 250 and 290°C. They also performed pure gas permeation test of H_2 and CO together with the binary mixture tests with 50% H_2, 50% CO and 50% H_2, 50% CO_2 fractions. Pure gas test showed H_2 permeance reducing from $3x10^{-5}$ mol/(m.s.Pa) to $1x10^{-5}$ mol/(m.s.Pa) while temperature decreases from 555 K to 500 K. Moreover, pure gas and binary mixture tests shown that H_2/CO selectivity decreases from approximately 40 to 30 when temperature increases from 200 to 290°C. Reaction tests shown that the best result, 95%, is achieved at 280°C and 400 kPa. Authors also found that CO_2 permeates through the membrane more compared to CO resulting in an additional positive effect on CO conversion. Lastly, it is found that permeation of CO to the permeate channel does not exceed the 2% of the inlet CO flow.

Araki et al. [32] used a silica membrane interlayered with γ-alumina on a α-alumina support to investigate WGS reaction in a membrane reactor. They used 0.5 g of commercial Pt catalyst at a temperature range of 250 - 350°C. Permeation tests involve pure gas tests where 20 mL/min Argon flow is used as the sweep gas in the permeate channel at 1.0 bar.

These pure gas tests for H_2, CO_2 and He shown that He has the highest permeance value compared to the other two gases. It is approximately equal to a value of $2x10^{-7}$ mol/(m^2.s.Pa) at 300°C and decreases approximately to $5x10^{-8}$ mol/(m^2.s.Pa) as temperature approaches 300 K. Additionally, H_2 permeance varies from $5x10^{-8}$ mol/(m^2.s.Pa) to $2x10^{-8}$ mol/(m^2.s.Pa) within the same temperature range. Permeances of each gas is also measured under WGS conditions. They are measured while steam to CO ratio is 2.0, GHSV is 1,800 $ml.h^{-1}$.g-cat^{-1} and pressures of retentate and permeate are equal to 200kPa to atmospheric pressure, respectively.

Table 2.3. Membrane parameters and H_2 purity found by Brunnetti et al. under WGS conditions.

	Permeances ($mol.m^{-2}.s^{-1}.Pa^{-1}$)			Selectivity		
Temperature (K)	H_2	CO_2	CO	H_2/CO_2	H_2/CO	H_2 purity (%)
523	$3.98x10^{-8}$	$2.08x10^{-11}$	$1.80x10^{-11}$	1920	2210	99.91
573	$5.38x10^{-8}$	$5.28x10^{-11}$	$1.80x10^{-11}$	1020	2990	99.81
623	$4.92x10^{-8}$	$5.52x10^{-11}$	$1.80x10^{-11}$	891	2730	99.79

Reaction tests are resulted with the membrane parameters and permeate H_2 purity given in Table 2.3. In terms of balancing between H_2 recovery and CO conversion, best results are gathered when steam to CO ratio is 2.0, pressure is 200 kPa and GHSV is 1800 $mL.h^{-1}$.CO conversion and H_2 recovery at these conditions were 99% and 50%, respectively.

Zhang et al. [33] investigated the low temperature WGS reaction with $CuO/ZnO/Al_2O_3$ catalyst in the presence of MFI zeolite membranes with modified zeolitic pores. These modifications are performed by on-stream catalytic cracking deposition (CCD) using methyldiethoxysilane (MDES). MDES is deposited through a 152 kPa flow that is prepared by mixing 40 cm^3 (STP)/ min equimolar H_2 and CO_2 with 5 cm^3 (STP)/ min Helium flow that contains MDES at 9 kPa partial pressure and 500 °C. Permeate flow was pure 30 cm^3 (STP)/ min He at atmospheric pressure during the modification. Under these flow conditions, H_2 permeance is found as $2.46x10^{-7}$ mol/ (m^2.s.Pa) with 38.8 H_2/CO_2 separation factor.

After bringing the pressure to atmospheric pressure and removing MDES from the flow, H_2 permeance and separation factor increase to $2.82x10^{-7}$ mol/m^2.s.Pa and 42.2, respectively. Permeation tests are also performed at the temperature range of typical low temperature WGS reaction, which is 150-300°C. H_2 permeance is changed from $8.0x10^{-8}$ mol/m^2.s.Pa to $1.6x10^{-7}$ mol/m^2.s.Pa when temperature is increased from 150 to 300°C. H_2/CO_2 separation factor is also changed from 7.0 to 21 in this temperature range with increasing temperature. Lastly, 95.4% conversion is achieved at 300°C through various parameter analysis performed by the authors.

Tang et al. [34] investigated the similarly prepared MFI zeolite membrane at high temperature WGS conditions. Binary mixture permeation tests are performed. WGS reaction is performed between 400 and 550°C with 200 mg Fe/Ce catalyst. The employed a pressure profile that drops from $1.517x10^5$ Pa to $1.013x10^5$ Pa (1.0 atm) for the reaction channel whereas pressure is kept at atmospheric pressure for permeate channel. Inlet flow of the reaction channel comprised only H_2O and CO and steam to CO ratio is varied between 1.0 and 3.5. Pure N_2 gas is employed in the permeate channel as the sweep gas. They test the H_2 permeance and H_2/CO separation factor at various stages such as pre and post modification of the membrane and before and after the WGS reaction using single and WGS mixture gases. H_2 permeance takes its highest value $4.21x10^{-7}$ mol/m^2.s.Pa at 550°C during a single gas test that has performed on unmodified membrane but has a relatively low perm selectivity (4.4) under these conditions. It takes its lowest value when the modified membrane is employed on the post-WGS reaction tests and binary mixture of H_2 and CO_2 is used as the test flow. H_2 permeance is inherently reduces in binary mixture studies due to the hindrance of larger and slower CO_2 on the permeation H_2. As a result, $1.21x10^{-7}$ mol/m^2.s.Pa H_2 permeance is acquired at 550°C and it reduces approximately to the $5x10^{-8}$ mol/m^2.s.Pa at 400°C under otherwise the same conditions. Separation factor also reduces from 37.3 to a value around 30 as temperature decreases from 550°C to 400°C. They also performed activity tests and parameter analysis of WHSV, sweep flow rate and steam to CO ratio. In the end, 81.7% conversion is achieved using a flow with properties of 60,000 h^{-1} WHSV, 1.0 steam to CO ratio, at 5.0 cm^3/min. Higher conversions (up to 100% conversion almost) are also achieved by decreasing WHSV and increasing steam to CO ratio but significant bypass of the equilibrium conversion is achieved in this particular arrangement.

Yin et al. [35] constructed a WGS reactor that uses $Cu/Zn/Al_2O_3$ as catalyst and Metal Organic Framework (MOF) based Zeolite Imidazolate Framework-8 (ZIF-8) as the membrane material. ZIF-8 is advantageous material since it has relatively high H_2 permselectivities and permeances and it can be prepared at benign conditions at a low cost. Permeation test is performed by both using single gas streams and syngas mixture that comprised 50 vol% H_2, 25 vol% CO, and 25 vol% CO_2. Single gas tests are performed at room temperature under 15 psi pressure. In mixed gas tests, syngas mixture is sent at 75 mL/min at 15 psi and 25 mL/min Argon used as the sweep gas at the retentate side. Single gas permeation tests resulted in $9.2x10^{-7}$, $1.5x10^{-7}$ and $2.3x10^{-7}$ mol/m^2.s.Pa for H_2, CO and CO_2, respectively giving 6.13 H_2/CO selectivity. In mixed gas tests, permeances reduces to $6.2x10^{-7}$, $1.2x10^{-7}$, and 1.8×10^{-7} mol/m^2.s.Pa for H_2, CO, CO_2, respectively resulting in 4.92 H_2/CO separation factor. Reaction tests are performed at 120-220°C temperature range at 40 L (STP)/g_{cat}.h. GHSV. At 220°C CO conversions is found approximately 40%, which is approximately the 20% more than the PBR result. In the presence of the reaction, H_2 permeance increased from $1.5x10^{-7}$ mol/m^2.s.Pa (H_2/CO separation factor is 1.3) to $3.3x10^{-7}$ mol/m^2.s.Pa (H_2/CO separation factor is 4.13) as temperature is increased from 120°C to 220°C. The reduction permeances compared to mixed gas tests are attributed to the inhibition coming from the moisture due to the presence of steam in the mixture. Lastly, stability of the membrane is investigated by single gas permeation tests and after 72 h exposure gas permeances are increased to $21.3x10^{-7}$, $5.9x10^{-7}$, and $6.8x10^{-7}$ mol/ m^2 s Pa, for H_2, CO and CO_2 respectively, which corresponds to 3.61 H_2/CO permselectivity.

Li et al. [36] investigated the ZIF-7 membrane in terms of mainly the hydrogen separation. Single gas measurements are performed at 1 bar with 50 mL/min test flow and N_2 is used as the sweep gas. For the binary gas mixture tests, 50 mL/min from each gas is used and each channel pressure is kept at 1.0 bar. Temperature is set to the 220°C in both single gas and binary mixture gas tests. As a result of single gas tests, H_2 permeance and CO_2 permeance are found as 4.55 $x10^{-8}$ mol/ m^2.s.Pa and $3.5x10^{-9}$ mol/ m^2.s.Pa, respectively. In mixed gas tests that involves equimolar binary mixture of H_2 and CO_2, H_2 permeance was still found as $4.55x10^{-8}$ mol/ m^2.s.Pa and CO_2 permeance slightly reduced to $3.3x10^{-9}$ mol/ m^2.s.Pa, which is not the usual case in many works in the literature. Authors also investigated the temperature effect and H_2 concentration on the membrane performance.

Based on the same binary mixture tests performed in the temperature range between 50°C and 220°C, activation energy of the membrane is found as 11.9 kJ/mol once the temperature profile data fitted to an Arrhenius type equation. Moreover, no significant change is observed in the permeance of CO_2 in this temperature range. H_2 concentration test are also resulted in no significant change in both CO_2 and H_2 permeance, except a slight increment to approximately $5x10^{-8}$ mol/m^2.s.Pa permeance when H_2 fraction was 0.1. Lastly, authors tested the hydrothermal stability of the membrane by employing 3% steam to the same binary mixture gas at 220°C testing the permeance of the membrane for 55 hours. Due to the presence of steam, slight reduction is observed in H_2 permeance but after 55 hours, H_2 permeance increased to 10% percent of its initial value of 4.55 $x10^{-8}$ mol/ m^2.s.Pa. Since similar behavior is also observed for CO_2, separation factor is maintained 13.6 during the 55 hours process.

Huang et al. [37] designed a ZIF-95 membrane and investigated its ability to separate H_2 from CO_2. Both single gas and equimolar binary mixture gas test are performed at 325°C and 1.0 bar with N_2 sweep gas. In single gas tests, H_2 permeance is found as 2.46 $x10^{-6}$ mol/ m^2.s.Pa and 34.9 ideal H_2/CO_2 separation factor. Single gas permeance order is found as $H_2 > N_2 > CH_4 > CO_2 > C_3H_8$ which is also confirmed by the DFT simulation to analyze the gas adsorption quality of the membrane. In binary gas mixture that contains H_2 and CO_2, Measured H_2 and CO_2 permeance is found as 1.95 $x10^{-6}$ mol/ m^2.s.Pa and 7.59 $x10^{-8}$ mol/ m^2.s.Pa, resulting in a separation factor of 25.7. Additionally, stability tests that are performed at 325°C and 1.0 bar shown that both H_2 and CO_2 permeance can approximately be kept at the same values after 24 h of operation. Lastly, hydrothermal stability of the membrane is evaluated by sending 3mol% of steam at 325°C and 1bar together with binary gas mixture and again H_2 permeance can is managed to kept at a slightly less permeance value, approximately $1.8x10^{-6}$ mol/ m^2.s.Pa, for 24 h operation.

2.3. Reaction Kinetics

Due to the various possibility of catalyst selection and reaction conditions employed in the studies, reaction mechanisms, therefore kinetic expression and parameters such as pre-exponential factors, activation energy and adsorption coefficients are expected to change from study to study. However, scientists also tried to express the kinetic relations through more general models such as Langmuir Hinshelwood model and Redox mechanism model to be able to express the kinetics in wider spectrum of conditions but in the end, many different and relatively complicated kinetic expressions are derived by scientists via reaction mechanism studies performed in molecular level. Therefore, utilizing simpler kinetic expressions and presenting corresponding parameter values found by empirical investigations in a limited temperature and pressure conditions is also very common method used in the literature. Below, several WGS reaction studies that involves different catalysts, kinetic expressions and resulting parameter values are summarized and important results and data are presented.

Amadeo et al. [38] investigated the kinetics of the low temperature WGS reaction catalyzed by 0.4 g $Cu/ZnO/Al_2O_3$ between 180°C and 230°C at atmospheric pressure. Experiments were conducted at constant temperature, with each gas's inlet partial pressure varied individually while maintaining constant partial pressures of the other components. To accommodate the changing fraction of gases to keep partial pressure constant, N_2 is used as the balance gas. 5 model equation that are fitted gathered from experiments are given in the order as

$$r = \frac{k.P_{H_2O}\,(1-\beta)}{A.P_{H_2O} + P_{CO}}, \tag{2.1}$$

$$r = \frac{k_1 k_2.P_{CO}P_{H_2O}\,(1-\beta)}{k_1.P_{CO} + k_2.P_{H_2O} + k_3.P_{CO_2}}, \tag{2.2}$$

$$r = \frac{k.P_{CO}P_{H_2O}\,(1-\beta)}{\left(1 + K_{CO}.P_{CO} + K_{H_2O}.P_{H_2O} + K_{CO_2}.P_{CO_2} + K_{H_2}.P_{H_2}\right)^2}, \tag{2.3}$$

$$r = \frac{k.P_{CO}(1-\beta)}{1+\frac{K_{H_2}K_{CO_2}.P_{H_2}P_{CO_2}}{P_{H_2O}}+K_{H_2}.P_{H_2}+K_{H_2O}.P_{H_2O}+K_{CO_2}.P_{CO_2}}, \quad (2.4)$$

$$r = \frac{k.P_{CO}P_{H_2O}\,(1-\beta)}{1+K_{CO_2}.P_{CO_2}+K_{H_2}.P_{H_2}}, \quad (2.5)$$

where β is given as

$$\beta = \frac{P_{CO_2}P_{H_2}}{K_{eq}P_{CO}P_{H_2O}}. \quad (2.6)$$

In Equations (2.1) to (2.6), k_i, P_i, K_i stands for reaction rate constants, partial pressures, and adsorption equilibrium constants of component i, respectively. K_{eq} is the equilibrium constant of the reaction. It can be calculated from the Gibbs free energies of the reaction components but the expression calculated by Moe et al. [39] as

$$K_{eq} = \exp\left(\frac{4577.8}{T} - 4.33\right) \quad (2.7)$$

is very widely used in the literature.

Equation (2.1) and (2.2), are the kinetic expressions derived for redox mechanism and Equation (2.3), (2.4), (2.5) are the kinetic expressions derived for Langmuir Hinshelwood mechanism. Equation (2.3) and (2.4) considers the adsorption of all four reaction gases and Equation (2.5) only considers the adsorption CO and CO_2. Equation (2.3) considers the surface reaction as the critical step and Equation (2.4) considers the CO adsorption as the critical step. As a result of the experimental analysis, scientists found that experimental results fitted best to the Equation (2.3). The resultant values of the parameters given in Equation (2.3) with respect to temperature are found as

$$k = 0.92e^{\left(-\frac{454.3}{T}\right)}, \quad (2.8)$$

$$K_{CO} = 2.2e^{\left(\frac{101.5}{T}\right)}, \quad (2.9)$$

$$K_{H_2O} = 0.4e^{\left(-\frac{158.3}{T}\right)}, \quad (2.10)$$

$$K_{CO_2} = 0.0047e^{\left(-\frac{2737.9}{T}\right)}, \quad (2.11)$$

$$K_{H_2} = 0.05e^{\left(-\frac{1596.1}{T}\right)}. \quad (2.12)$$

The reaction is performed on Pt catalysts that are supported on ceria and alumina under typical conditions of fuel reformers for fuel cell applications. To reflect that accurately, experimental data are gathered by using an inlet gas mixture consisted of 6.8% CO, 8.5% CO_2, 22% H_2O, 37.3% H_2, and 25.4% Ar, at a total pressure of 1 atm, over the temperature range of 180 - 345°C. They expressed reaction kinetics in an empirical power rate law equation given as

$$r = k.{C_{co}}^{a}\,{C_{co_2}}^{b}{C_{H_2}}^{c}{C_{H_2O}}^{d}(1-\beta). \quad (2.13)$$

β is equal to the same expression given in Equation (2.6). Reaction orders of each component [a, b, c, d in Equation (2.13)] and activation energies of the reactions performed on each catalyst are also calculated by the authors. Authors also tries express the kinetic model through seven-steps redox mechanism and modified redox mechanism with the help of diffuse reflectance infrared Fourier transform spectroscopy (DRIFTS) but reaction mechanism and intermediates cannot be effectively clarified despite achieving quantitative consistency with both methods.

Table 2.4. Kinetic parameters for WGS reaction on Pt based catalysts.

			Reaction Order			
Catalyst	Activation energy (kJ/mol)	Temperature (°C)	CO	CO_2	H_2	H_2O
1%Pt/Al_2O_3	64	285	0.06	-0.09	-0.44	1.0
1%Pt/Al_2O_3	84	315	0.1	-0.07	-0.44	1.1
1.66%Pt/Al_2O_3	81	285	0.11	-0.06	-0.49	0.82
1.66%Pt/Al_2O_3	81	300	0.1	-0.08	-0.46	0.77
1%Pt/CeO_2	75	200	-0.03	-0.09	-0.38	0.44

Hla et al. [41] investigated the kinetics of high temperature water gas shift reaction performed on two different copper promoted iron chromium based commercial catalysts.

Temperature range is maintained at 360 - 450°C range and pressure is taken as constant atmospheric pressure. Additionally, space velocity is adjusted to 1.9 $m^3.g_{cat}^{-1}.h^{-1}$. Two catalysts differentiate from each other in terms of chromium and copper fractions. First catalyst, HTC 1, contains slightly higher fraction of chromium and second catalyst, HTC 2, contains slightly higher copper fraction. Both catalysts' weight also kept at 0.2 g in each experiment. Authors also tested the activity of the catalyst using four different inlet streams that have varying gas fraction but performed the kinetic analysis using a flow that have 65% CO, 30% H_2, 2% CO_2 and 3% N_2 dry gas fractions. In addition to these gases, water pumped at a rate of 1.288 mL/min (8% of CO_2 flow) turned into steam and added to the reaction. Authors used a power rate law expression given in Equation (2.13). The reaction rate found for HTC 1 is given as

$$r = 10^{2.845} e^{\left(-\frac{-111000}{8.3144T}\right)} P_{CO} {P_{CO_2}}^{-0.36} {P_{H_2}}^{-0.09} \left(1 - \frac{P_{CO_2} P_{H_2}}{K_{eq} P_{CO} P_{H_2O}}\right), \quad (2.14)$$

and for HTC 2, it is given as

$$r = 10^{0.659} e^{\left(-\frac{-88000}{8.3144T}\right)} {P_{CO}}^{0.9} {P_{H_2O}}^{0.31} {P_{CO_2}}^{-0.156} {P_{H_2}}^{-0.05} \left(1 - \frac{P_{CO_2} P_{H_2}}{K_{eq} P_{CO} P_{H_2O}}\right). \quad (2.15)$$

3. MATHEMATICAL MODELING

The initial calculations for validation purposes of ZIF-7 membrane model with Cu/Zn catalyst follow the geometric model outlined in Lee et al.'s work [42], which stands as a rare experimental test of a ZIF-7 membrane under actual WGS reaction conditions. In this model, ZIF-7/Mg-Al_2O_3 membrane divides the reactor into two concentric cylinders and it has inside and outside diameters of 7.0 mm and 10 mm, respectively. Between the cylindrical membrane and the outer wall that have 14 mm inside and 16 mm outside diameter, respectively, a typical Cu/Zn catalyst for low-temperature WGS reaction, weighing 2.26 g, is packed. The 30 mm reactor length reported by Lee et al., is utilized to calculate bed density and inlet molar flow rate, which is determined as

$$F_{total} = GHSV * V_R * 22.4\ mol.L^{-1} \tag{3.1}$$

in standart conditions and computed as 8.08×10^{-2} mol/h with appropriate unit conversions.

Similar to the Cu/Zn model, parameters related to the inlet flow and the microchannel reactor for Pt-CeO_2 catalyst model are derived from the geometric setup as described by Germani and Schuurman [43], which has also been utilized in a previous study [16]. These investigations revolve around modeling the WGS reaction within an adiabatic microchannel reactor and the earlier work [16] additionally explores the feasibility of achieving isothermal conditions by employing neighboring microchannels as cooling channels. The primary reactor, spanning 5×10^{-2} m in length, features a rectangular cross-section with dimensions of 4×10^{-4} m in height and 6×10^{-4} m in width. A thin layer of Pt-CeO_2 catalyst, with a thickness of 5×10^{-5} m, is assumed to be coated at the retentate side wall of this rectangular prism reactor. Furthermore, a ZIF-7 membrane is incorporated as the upper wall of the reactor geometry, dividing the reactor into permeate and retentate sides. For validation studies, the inlet molar flow rate is determined as 2.53×10^{-7} mol.s^{-1}, derived from the reported volumetric flowrate value of 5.67×10^{-9} $Nm^3.s^{-1}$ elsewhere [16]. The washcoat density of Pt-CeO_2 is taken as 1.45×10^3 kg.m^{-3} based on the data provided by Germani and Schurmann [43] and 22.4 m^3 volume of 1 kmol of ideal gas in STP conditions is accounted for this calculation.

Subsequently, the weight of Pt-CeO_2 catalyst, amounting to $2.16x10^{-6}$ kg, is computed considering the bed density and the assumed washcoat thickness of $5x10^{-5}$ m. [16]

The conventional WGS adiabatic process is simulated by modeling Fe-Cr and Cu/Zn based catalysts in a similar fashion by setting the mass transfer through the membrane as zero in the same reactor geometry. Bed density is taken as the same value to eliminate a potential cause of difference in other parametric studies.

The choice of a ZIF-7 membrane for both models is based on its good thermochemical stability with MgO support at 300°C [44], and can be further extends to the 400°C with the Mg-Al_2O_3 support [42] aligning with the typical temperature range for the high-temperature water gas shift reaction and enabling its usage for Pt-CeO_2 catalyst model. Furthermore, its capacity for steam transfer, often considered undesirable, enables higher CO conversion rates by introducing the reverse permeation of steam from the permeate channel to the retentate channel.

As per Lee et al. the inlet composition is modeled to mirror the output of a steam methane reforming reactor. Therefore, the inlet fractions are set to 7% CO, 21% H_2O, 26% CO_2, and 46% H_2 in Cu/Zn catalyst model. The bed density, calculated at 0.999 $g.cm^{-3}$ based on the provided catalyst weight and reactor dimensions, aligns closely with the given approximate value of ~1.0 $g.cm^{-3}$. On the other hand, inlet flow in Pt-CeO_2 catalyst comprises 10% CO, 20% H_2O, 10% CO_2, 30% H_2 and 30% Ar with the aim of reflecting the fractions observed post-outlet of a gasoline autothermal reformer supplemented by a steam stream [45].

Lee et al. reported the gas permeance data with respect to temperature in both equation form and in a graphical depiction for the ZIF-7 membrane. However, upon computation, a discrepancy emerged between results derived from the equations and those illustrated in the figure. Consequently, calculations are based on the gleaned values from figure expressed as a temperature function using exponential fitting. Resultant equations are found as

$$Pe_{H_2} = 4.68 * 10^{-7} * exp\,(4.26 * 10^{-4} * T), \qquad (3.2)$$

$$Pe_{H_2O} = 1.96 * 10^{-8} * exp\,(3.97 * 10^{-3} * T), \quad (3.3)$$

$$Pe_{CO} = 7.52 * 10^{-8} * \exp(1.28 * 10^{-3} * T), \quad (3.4)$$

$$Pe_{CO_2} = 2.46 * 10^{-8} * exp(2.36 * 10^{-3} * T). \quad (3.5)$$

In this analysis, alternative equation fitting methods are also examined, revealing no notable impact. (The change in CO conversion is less than 0.5%).

Tosti et al. [46] provide H_2 permeance data for Pd-Ag membrane in the form of Arrhenius Equations, intended for use in membrane comparison in Cu/Zn catalyst model. The resultant equations are

$$Pe_{H_2} = 7.2 * 10^{-4} * exp\left(-\frac{1866.6}{T}\right), \quad (3.6)$$

$$Pe_{H_2} = 5.8 * 10^{-5} * exp(-521.0/T). \quad (3.7)$$

Equations (3.6) and (3.7) are specified for temperature ranges of 135-275°C and 275-360°C, respectively. In Pd-Ag membrane model, the geometric structure of the membrane remains constant as the way it is introduced with the ZIF-7 case, with the only alteration being the substitution of data related to permeance and permeation fluxes.

Permeation flux is determined utilizing Sievert's Law for Pd-Ag membrane and it is expressed as

$$J_{H_2,Pd} = Pe_{H_2}\left(\sqrt{P_{H_2,retentate}} - \sqrt{P_{H_2,permeate}}\right) * \frac{3600\ s}{1\ h}. \quad (3.8)$$

However, since the units of permeance data are in $mol.m^{-2}.s.Pa^{-1}$ for ZIF-7, corresponding permeation fluxes are computed via the equation given as

$$J_{i,ZIF-7} = Pe_i\left(P_{i,retentate} - P_{i,permeate}\right) * \frac{3600\ s}{1\ h} \quad (3.9)$$

to obtain the flux value in correct units. Since ZIF-7 membrane is common in both Pt-CeO_2 and Cu/Zn catalyst models, permeation fluxes are simulated in both models using Equation (3.9) without any change.

The initial validation studies in Cu/Zn model are conducted by modeling a 1D steady-state isothermal reactor in a counter-current flow configuration, with the inlet temperature varying between 225°C and 325°C. A sweep gas, comprising 0.134 mol. h^{-1} of Argon, flows through the permeate side, and the pressure is maintained at 1 bar in both the retentate and permeate channels. However, the flow arrangement is later modified to co-current flow, with the sweep molar flow rate adjusted to 1.072 mol.h^{-1} and the pressure in both channels set to 10 bars, based on the insights gained from further analysis. The rationale behind these adjustments is outlined in the "results and discussion" section.

Pt-CeO_2 catalyst operation is modelled in a 1D steady-state isothermal reactor in a co-current flow arrangement for the validation phase, since the operation presented in previous work [16] occurs in co-current arrangement. Due to the advantages of co-current operation that are observed in Cu/Zn model, co-current arrangement is kept as the default setting for further analysis. In this model, however, the pressure and temperature range are initially established at 1 bar and 200 - 320°C, respectively, to align accurately with literature data. Subsequently, the temperature range and pressure are extended to 350-450°C range in simulations representing conventional high-temperature adiabatic WGS reaction, but ultimately, the process with a 350°C inlet temperature is selected for representation. Following this, low-temperature WGS reaction is modeled at both 200° and 250°C inlet temperature and pressure maintained constant at 10 bar for both HT and LT-WGS reactions. In the membrane model, the temperature range is defined as 200 – 400°C, while pressure alternates between 1-5-10 bar. Sweep gas flow alternated between Argon or steam flows, with magnitudes set at 10 or 50 times the inlet retentate molar flowrate.

The catalysts employed in the experimental studies conducted by Lee et al. are synthesized by the authors themselves. In order to reasonably approximate the reaction kinetics observed in their studies in Cu/Zn catalyst model, Cu/ZnO/Al_2O_3 reaction kinetic data are adopted from Choi and Stenger [46] and are represented as

$$-r_{CO,Cu/ZnO} = k_{Cu/ZnO} * \left(P_{CO} P_{H_2O} - \frac{P_{CO_2} P_{H_2}}{K_{eq}} \right), \quad (3.10)$$

$$k_{Cu/ZnO} = 2.96 * 10^5 * exp\left(\frac{-47400}{RT}\right). \quad (3.11)$$

Further discussion in section 4.1.1 delves into potential implications of this variance. These kinetic data are also used in modelling the membraneless low temperature WGS reaction to compare membrane microreactor with Pt-CeO_2 catalyst with conventional process.

In addition to the Cu/ZnO/Al_2O_3 catalyst, microreactor model with Pt-CeO_2 catalyst requires kinetic expressions for a Pt-CeO_2 catalyst and an Fe-Cr catalyst. These kinetic expressions and required parameter data are given as

$$-r_{CO,Pt\_CeO_2} = \frac{k_{Pt\_CeO_2} * K_{CO}K_{H_2O}P_{CO}P_{H_2O}\left(1 - \frac{P_{CO_2}P_{H_2}}{K_{eq}P_{co}P_{H_2O}}\right)}{\left(1 + K_{CO}P_{CO} + \sqrt{K_{H_2}P_{H_2}}\right)^2\left(1 + K_{CO_2}P_{CO_2} + \sqrt{K_{H_2O}P_{H_2O}}\right)}, \quad (3.12)$$

$$k_{Pt\_CeO_2} = 3.7 * 10^7 * exp\left(\frac{-78200}{RT}\right), \quad (3.13)$$

$$-r_{CO,Fe-Cr} = k_{Fe-Cr} * P_{CO}P_{CO_2}^{-0.6}P_{H_2O}^{0.25}\left(1 - \frac{P_{CO_2}P_{H_2}}{K_{eq}P_{co}P_{H_2O}}\right), \quad (3.14)$$

$$k_{Fe-Cr} = 8.159 * 10^7 * exp\left(\frac{-114600}{RT}\right). \quad (3.15)$$

Equations (3.12) – (3.13) [16] and (3.14) – (3.15) [47,48] are employed for Pt-CeO_2/Al_2O_3 and commercial Fe-Cr based catalyst, respectively. Equations (3.10), (3.12) and (3.14) define $-r_{CO}$ as the rate of CO consumption, while P_i represents the partial pressure of component i in bars. However, in Equation (3.14), the unit is converted to atm. The partial pressures of each component are calculated using Raoult's Law for every catalyst. Additionally, the values of adsorption constants, K_i, in Equation (3.12) can be sourced from elsewhere [43].

The models make several assumptions that need to be considered when evaluating the results. Firstly, the streams in both channels are treated as an ideal and incompressible fluid and axial diffusion is disregarded in both models due to the high inlet velocity of the retentate gas (~6.7 m/s) in Cu/Zn model and high Length/Diameter ratio of the microreactor in Pt-CeO_2 catalyst model. Additionally, due to the laminar flow condition within the microreactor and relatively short lengths of both models, momentum balances are also neglected.

Any diffusion limitations on the reaction, as well as additional side reactions and homogeneous reactions are disregarded. In Cu/Zn catalyst model, overall heat transfer coefficient in energy balances are held constant within the range of 200 – 500 W/(m^2.K) for non-isothermal cases. The examination of these findings indicates that isothermal conditions can be succeeded across the reactor except for an initial hotspot. Consequently, the differential equation governing the energy balance is automatically set to zero for subsequent isothermal simulations and Pt-CeO_2 catalyst model.

Modelling tasks are carried out using MATLAB 2023A, with the differential equations governing mass and energy balances given as

$$\frac{dF_{i,R}}{dw_{cat}} = v_i r - \frac{J_i S_m}{\rho_b}, \tag{3.16}$$

$$\frac{dF_{i,P}}{dw_{cat}} = \frac{J_i S_m}{\rho_b}, \tag{3.17}$$

$$\frac{dT_R}{dw_{cat}} = \frac{\frac{US_m}{\rho_b}(T_P - T_R) - r.\Delta H_{rxn}}{\sum F_{i,R} C_{p,i}}, \tag{3.18}$$

$$\frac{dT_P}{dw_{cat}} = \frac{\frac{US_m}{\rho_b}(T_R - T_P)}{\sum F_{i,P} C_{p,i}}, \tag{3.19}$$

$$\frac{dT_R}{dw_{cat}} = \frac{-r.\Delta H_{rxn}}{\sum F_{i,R} C_{p,i}} \tag{3.20}$$

are solved via ode45 function. Equation (3.16) and Equation (3.17) represent the mass balances applied to the retentate and permeate channels, respectively, in a co-current arrangement. In instances where membranes are not present, the second term associated with the transfer of each component through the membrane is excluded from Equation (3.16), while Equation (3.17) is taken as equal to zero. Equation (3.18) and Equation (3.19) are employed to compute the energy balances for the retentate and permeate channels under non-isothermal conditions in Cu/Zn model, respectively. In adiabatic simulations used in Pt-CeO_2 model, Equation (3.20) is utilized to determine the temperature profile within the retentate channel, while the rate of change of temperature within the permeate channel is set to zero.

Reaction enthalpy in Equation (3.18) and (3.20) is modified based on the reactor temperature by integrating the heat capacities of each component over the temperature range from room temperature to the channel temperatures. The resulting value is then added to the reaction enthalpy at room temperature, taking into account the reaction stoichiometry.

Counter-current calculations performed in Cu/Zn model involve an iterative process where the output of the permeate channel is estimated initially and then used as the initial values for the permeate channel variables. This approach ensures that mass and energy transfer between the two channels occurs at adjacent zones in each iteration, as ode45 is utilized. Consequently, for counter-current arrangements, the permeate channel variables are recalculated from outlet to inlet. Equations that are given as

$$\frac{dF_{i,P}}{dw_{cat}} = -\frac{J_i S_m}{\rho_b}, \tag{3.21}$$

$$\frac{dT_P}{dw_{cat}} = -\frac{\frac{US_m}{\rho_b}\,(T_R - T_P)}{\sum F_{i,P} C_{p,i}} \tag{3.22}$$

are used instead of Equation (3.16) and Equation (3.18), respectively.

The process is reiterated until the desired inlet conditions for the permeate channel are met. This approach is preferred over employing boundary value problem solvers, as counter-current studies are solely utilized for validation purposes. Consequently, the iterative method of guessing the suitable output conditions is discovered to be less time-consuming than utilizing a boundary value solver.

When employing Equation (3.21) and Equation (3.22) as described earlier, a minor assumption is necessary. Permeation fluxes, molar flow rates, and heat capacities are computed based on the temperature and partial pressure values further along the path of the permeate flow. While this approach does not precisely mirror the actual interaction between the two channels, where previous interactions naturally influence the parameters of subsequent points, it is considered acceptable for counter-current flow calculations. The reason behind it is the fact that the "step-size" of the ode45 solver is exceptionally small.

This is due to the high absolute and relative tolerances employed in the calculation (10^{-10}), effectively minimizing the impact of the previously stated effect.

4. RESULTS AND DISCUSSION

Validation of the model are performed by comparing the membrane and non-membrane CO conversion results to the data gathered from literature and previous works. Following that, the effect of sweep gas type and molar flow rate are studied in the membrane enabled models. Effect of channel pressure are also investigated for both catalysts. In the model with Cu based catalyst, ZIF-7 membrane results are compared to the results gathered from Pd membrane and effect of gas hourly space velocity (GHSV), flow arrangement (co- or counter current) and validity of isothermal conditions are investigated. In the model with Pt-CeO_2 catalyst, additionally, effect of residence time is investigated and CO conversion results gathered from the most optimal systems is compared to the conventional two-reactor adiabatic WGS system model that is widely used in chemical industry.

4.1. WGS Modelling on Cu/Zn Based Catalyst

4.1.1. ZIF-7 Membrane Model Validation

The study's initial phase involves validating the model by comparing CO conversion with the data gathered from Lee et al.'s research. To get the appropriate results to compare with the Lee et al.'s results and ensure the correct validation of the data, model is configured in a counter-current setup, employing argon as the sweep gas in the permeate channel. In these runs, both channels are kept at 1 bar pressure and inlet sweep molar flow rate is taken as the default reported value 0.134 $mol.h^{-1}$ in Lee et al.. Resultant data are presented in Figure 4.1, showcasing CO conversion with respect to different isothermal temperature profiles ranging from 498 K to 573 K. Here, it is important the mention that since a kinetic data is not reported in the Lee et al.'s work, utilized kinetic data belonging to a commercial $CuO/ZnO/Al_2O_3$ catalyst is taken from the work of Choi and Stenger [46]. Prior to the validation runs, this difference in catalysts was expected to cause a potential difference in the CO conversions at lower temperatures.

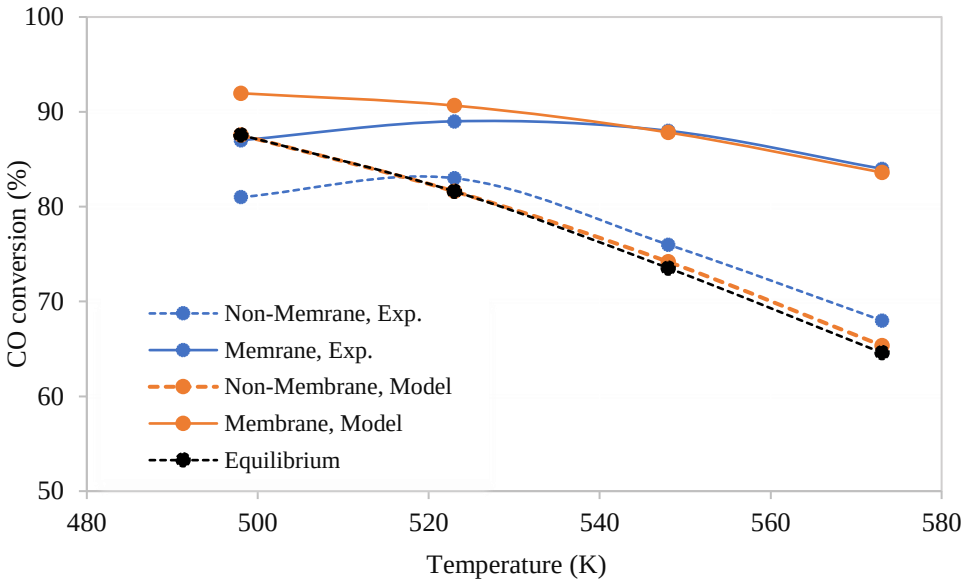

Figure 4.1. Temperature vs CO conversion, blue curves are the results found by Lee et al.[42].

Based on Figure 4.1, CO conversion values at 523 K and above exhibit consistent results with the experimental data gathered from Lee et al. Both studies accurately represent the equilibrium conversion for the non-membrane case. However, a minor disparity in the CO conversion value is also noticeable at 225°C in Figure 4.1 as expected.

As previously mentioned, it is quite likely that the activation energy and Arrhenius constant values used in our kinetic model do not perfectly align with the corresponding characteristics of the catalyst synthesized by Lee et al.'s. However, based on the result presented within 250-300°C range, this inequality does not seem to have a significant impact on CO conversion values as indicated by the similarity in the results given in Figure 4.1 due to the presence of equilibrium conditions in the non-membrane cases. Assuming there are not any experimental errors in the results of Lee et al., the discrepancy at 225°C might be explained by the utilization of faster reaction kinetics gathered from Choi and Stenger proved by the overlapping result of non-membrane model scenario and non-overlapping result of non- membrane experimental scenario with the equilibrium curve.

In non-membrane applications, minimization of catalyst usage is one of the key factors in the reactor design so amount of catalyst used is adjusted so that equilibrium is just reached at the exit of the reactor. However, membrane reactors function differently in that sense since the component transfer through the membrane constantly disrupts the equilibrium, allowing higher conversion values beyond the equilibrium conversion. Thus, having higher catalyst mass (longer reactor geometry) in membrane reactors compared to the non-membrane reactors can be advantageous.

Employing 2.26 g of catalyst provides a situation where this phenomenon can be benefitted from. As it can be seen from Figure 4.2, even if the non-membrane reactor is operated under isothermal conditions at 225°C, equilibrium conditions are already achieved in the region close to the reactor inlet and residence time of the flow under equilibrium conditions is high. Also, this post-equilibrium section will be extended at higher temperatures since reaction is faster and equilibrium conversion is lower. This type of reactor is both the underlying reason for the conversion difference between the membrane and non-membrane scenarios since component transfer (mostly H_2) in this section adjust partial pressures of the components in a way that furthers the forward reaction, and also important for explaining the validity of the results for 250-300 °C range despite the possible difference in kinetic parameters governing the reaction between our model and Lee et al. Validity of these findings can be justified by the following reasoning: When reaction rates surpass mass transfer rates through the membrane by a significant margin, the influence of reaction kinetics diminishes notably since the limiting factor for CO conversion becomes the mass transfer through the membrane. Consequently, as long as the reaction rates are markedly high, the time required to achieve equilibrium conditions disrupted by component transfer remains relatively constant. This results in negligible difference in CO conversion, as presented in Figure 4.3. Thus, for 300 and 350°C where reaction rates are high, our model overlaps with the Lee et al. results in Figure 4.1 as expected and there is only a subtle difference in 250°C. This is probably due to the reaction rates getting slower and closer to the mass transfer rates through the membrane for experimental data. Hence, our model proves suitable for exploring the impact of a ZIF-7 membrane on the water-gas shift reaction, catalyzed by a Cu/Zn catalyst, using the kinetics provided in Choi-Stenger.

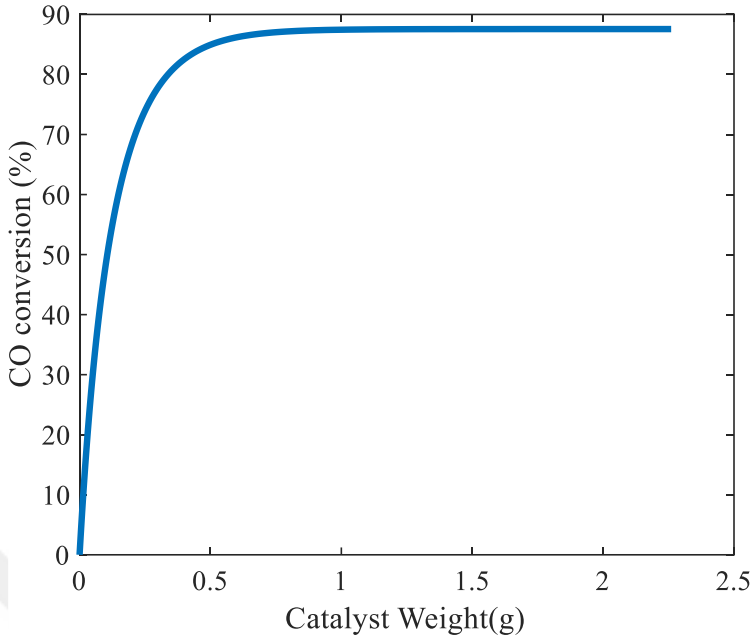

Figure 4.2. CO conversion for non-membrane case at 225°C, 1bar.

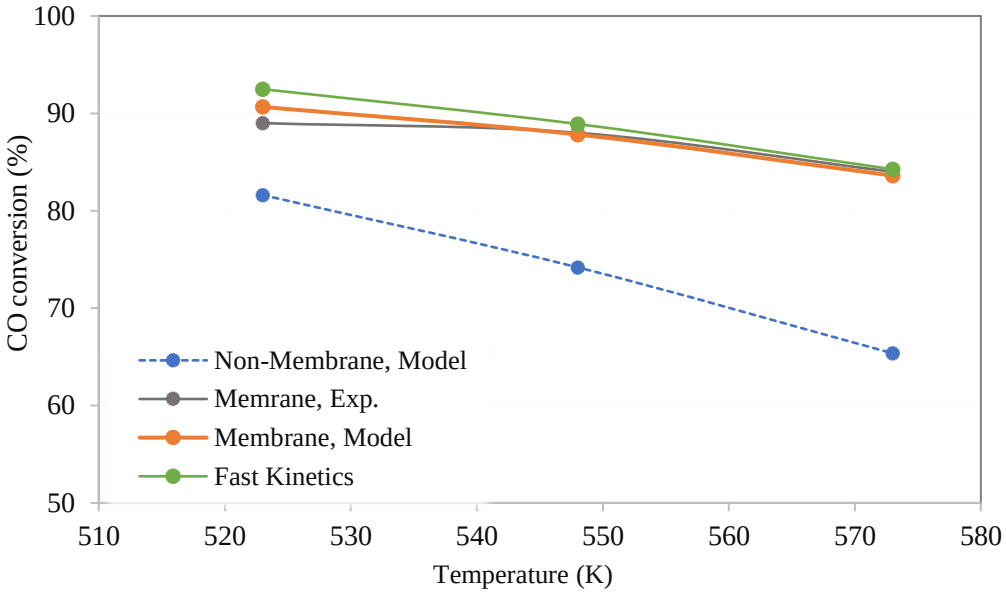

Figure 4.3. Fast kinetics CO results: Reaction kinetic is multiplied by 10^{18} arbitrarily.

4.1.2. Effect of Sweep Flow

After the validation studies, further analysis is conducted to examine how the flow arrangement, sweep gas type and the amount of steam used as the sweep gas impact the conversion of CO. Figure 4.4 and 4.5 displays the relevant results of this investigation.

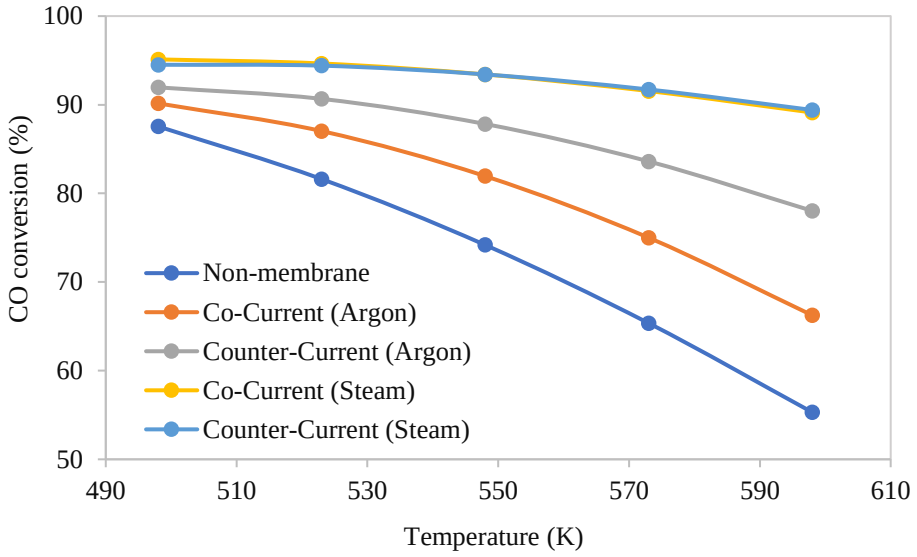

Figure 4.4. Effect of sweep flow type and arrangement, 0.134 $mol.h^{-1}$ sweep molar flowrate, 1 bar.

Looking at Figure 4.4, counter-current arrangement is more advantageous for CO conversion when employing Argon as the sweep gas. This can be explained by the fact that inlet and H_2-poor part of the sweep (permeate) flow interfaces with the H_2-producing equilibrium region in reaction (retentate) channel. Consequently, the difference in H_2 partial pressure between the two channels that acts as the driving force for H_2 transfer, is higher compared to the co-current flow arrangement. In contrast to the situation in counter current arrangement, H_2 fraction manages to reach higher rates in equilibrium region in co-current arrangement due to interfacing with H_2-rich outlet section of permeate channel and having reduced rate of H_2 transfer because of that. Hence, final CO conversion is lower compared to the counter current arrangement due to the lessened effect of Le Chatelier principle.

ZIF-7 not having infinite selectivity towards H_2 and its allowance for H_2O passage increases CO conversions in the models where steam is employed as the sweep gas. Having a decent permeance value at higher temperatures and being the single gas in the retentate channel causes a high rate of H_2O transfer through the membrane. The reverse transfer of steam elevates the partial pressure of steam in the retentate channel while simultaneously lowering the partial pressure of other gases. With the given kinetic in Equation (3.10), forward reaction is boosted by the elevated partial pressure of steam and at the same time CO loss to the permeate channel is partially mitigated by the lowered CO partial pressure. Consequently, using steam instead of Argon as the sweep gas in our model result in higher CO conversion, making it the default choice for the following studies.

Figure 4.4 also shows another important result. When steam is used as the sweep gas flow arrangement does not have any noticeable impact on CO conversion which can be stemmed from two reasons.

CO permeability of the membrane can be one of these reasons. As previously given in Equation (3.4), CO can pass through the ZIF-7 membrane so some amount of CO towards the inlet of the reactor will be inevitably lost to the permeate channel prior to entering the reaction. Consequently, maximum CO conversion that can be attained will be limited at a value under 100%. Also, this effect will be especially prominent at higher temperatures where equilibrium CO fraction is higher. CO conversion rates being close to or higher than 90% conversions for steam-as-a-sweep-gas models, it is likely that this conversion limits will be preventing CO conversion from changing when flow arrangement is changed.

The second reason is related to the changing influences on the forces that regulates H_2 and steam transfer through the membrane that depends on whether steam or Argon is used as the sweep gas. It is previously mentioned that the reverse permeation of steam also boosts the CO conversion in addition to the regular H_2 transfer. It is also mentioned that since residence time under equilibrium conditions is long at non-membrane cases, CO conversion is limited by the mass transfer through the membrane rather than reaction kinetics.

In the scenarios where Argon is employed as the sweep gas, steam transfer effect is not present and CO conversion solely depends on H_2 transfer. Since H_2 has the highest permeance value, any change on partial pressure difference relations between the channels induced by switching the flow arrangement will have significant impact on H_2 transfer. Because of the sole dependence of CO conversion on H_2 transfer, CO conversion increases by employing counter- current arrangement on the scenarios where Argon is the sweep gas. In the scenarios where steam is the sweep gas, transfer of the steam through membrane have more impact on CO conversion compared to the H_2 transfer, as it is proven by the higher CO conversion values in co-current steam scenario compared to the counter current Argon scenario in Figure 4.4. Since steam's permeance value is drastically lower than the permeance value of H_2, employing different flow arrangement have less impact on steam transfer rate through the membrane and hence CO conversion, which is consistent with results present in Figure 4.4.

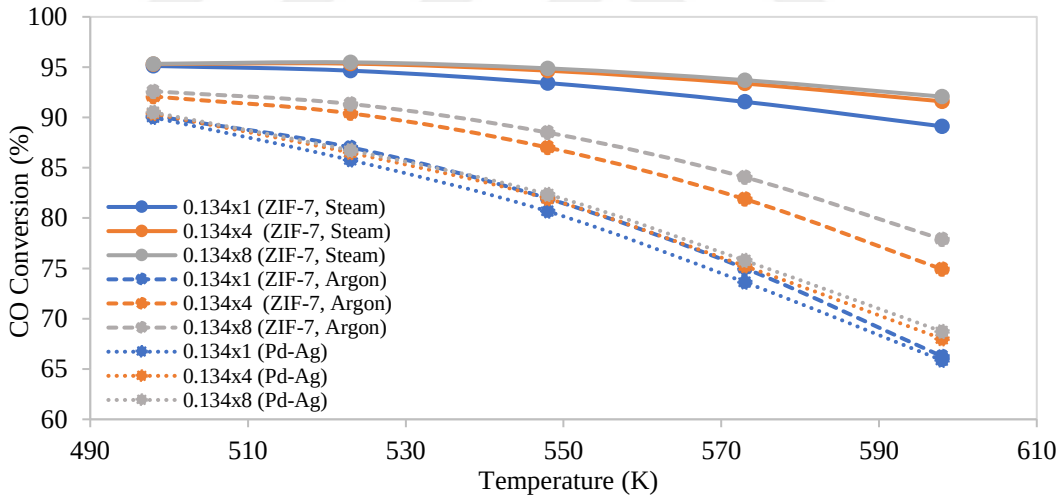

Figure 4.5. Effect of sweep flow rate on Pd-Ag and ZIF-7 membranes, 1 bar.

Figure 4.5 illustrates how altering the molar flow rate of the sweep gas in the permeate channel impacts the CO conversion in both Pd-Ag and ZIF-7 membrane models in a co-current configuration. Figure 4.5 demonstrates that as the molar flow rates of the sweep gas increase, there is a diminishing increase in CO conversion across all cases depicted. This outcome is anticipated because the partial pressure of each gas in the permeate channel increase at a slower rate per unit of permeated gas due to the increasing molar flowrate.

Consequently, CO conversion increases due to faster H_2 rate through the membrane boosting the effect of Le Chatelier principle. For the cases where steam is employed as sweep gas, reverse transfer of H_2O through the membrane is also increased since pressure of steam in permeate channel decreases slower due to the higher molar flowrate. Consequently, CO conversion also increases. However, as partial pressures approach zero during permeate flow, the differences in partial pressures of each component reach their maximum values. Consequently, further increase in the sweep flow rate have minimal impact on the system. Upon analyzing the results presented in Figure 4.5, it was determined that a sweep molar flow rate of 1.072 mol/h (equivalent to 0.134x8 mol/h) of H_2O is adequate for this purpose.

The previous analysis is valid for Pd-Ag applications as well. In our study, Pd-Ag membrane exhibits infinite selectivity towards H_2 but possesses a lower permeance value compared to ZIF-7. The lower conversion values observed in Argon sweep gas scenarios indicate that despite ZIF-7 permitting the passage of other species, the higher permeance of H_2 and the transfer of CO_2 still result in higher CO conversions in ZIF-7 membrane.

4.1.3. Co-current Flow and Isothermal Assumption

From the results given in Figure 4.5, 1.072 mol/h (0.134x8) steam in a co-current arrangement is selected as default sweep gas flow. Additionally, employing steam as the sweep gas yields the highest conversion rates, with no noticeable variation in CO conversion that stems from alternating between co-current and counter-current arrangement.

Since flow arrangement does not affect CO conversion in the default case, flow arrangement is determined so that isothermal process conditions can be achieved as much as possible. Figures 4.6 and 4.7 illustrates the temperature profiles for the co and counter current arrangement, respectively. Both processes depicted in Figure 4.6 and 4.7 is designed with the aim of achieving an isothermal profile for retentate channel at 275°C. To understand the interaction between channels easier, in Figure 4.7 (counter-current), axis value of 2.26 and 0 in orange curve corresponds to the inlet and outlet of permeate channel, respectively.

In Figure 4.6 and 4.7, occurrence of hot spot can be detected from the peak at the entrance of retentate channel even though the inlet temperature of the permeate channel adjusted to achieve isothermal profile. However, there is also a noticeable difference in magnitude in favor of the co-current flow, approximately 10°C less, between the hot spots that corresponds to the two-flow arrangement.

This difference in hot spot temperature arises because for the counter-current flow, minimal heat generation at the retentate channel outlet, where the reaction occurs at equilibrium conditions, prohibits setting the inlet temperature of the permeate flow to a significantly lower value from the targeted isothermal temperature since a significantly lower value swiftly decreases the temperature under the intended isothermal temperature within the retentate channel. Consequently, temperature exhibits an increasing pattern towards the outlet section of the permeate channel since this section interfaces with the inlet section of the retentate channel where heat generation is maximum due to the high reaction rate. So, rather that quenching the heat generation as in the case in co-current arrangement, permeate channel temperature elevates the hot spot temperature further compared to co-current arrangement, where freedom of setting the temperature of the permeate section that directly interfaces with the hot spot is available. Therefore, the default flow arrangement is selected as the co-current flow for further studies.

Additionally, validity of isothermal process assumption in the presence of hot spot is investigated by comparing the CO conversion values that corresponds to the curves illustrated in Figure 4.6 and 4.7 (94.92% and 94.99%, respectively.) with the data gathered from the simulations where Equation (3.18) - (3.19) are set to zero to succeed isothermal conditions arbitrarily. (94.88% co-current, 94.94%, counter-current). Given that the conversion varies merely around 0.5% between the corresponding configurations, the isothermal assumption appears to be a valid approximation for the present model.

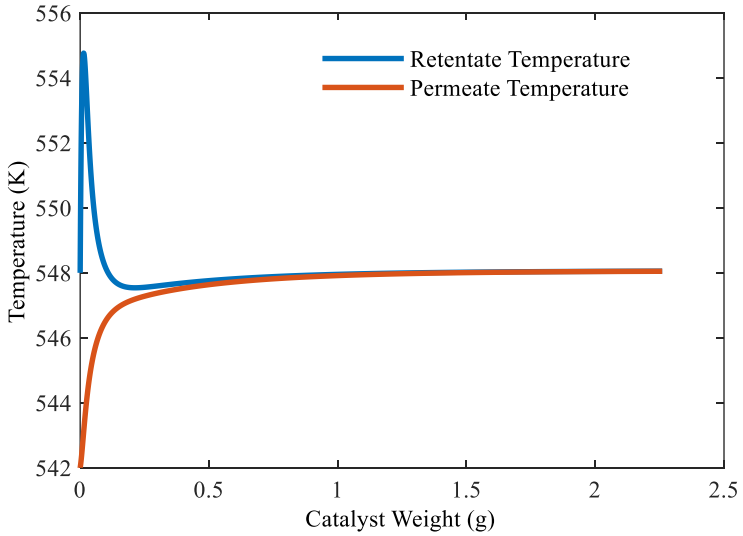

Figure 4.6. Temperature profile of the model for co-current arrangement. Blue curve and orange curve represent retentate and permeate channel, respectively. Overall heat transfer Coefficient (U) is chosen as 200 $W/m^2/K$, sweep flow is 1.072 $mol.h^{-1}$ $H_2O_{(g)}$, channel pressures are 1 bar.

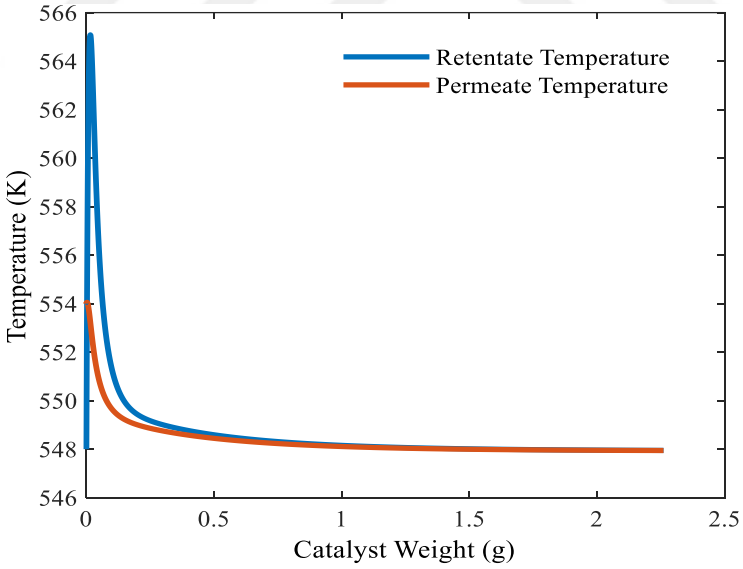

Figure 4.7. Temperature profile of the model for counter-current arrangement. Blue curve and orange curve represent retentate and permeate channel, respectively. Overall heat transfer Coefficient (U) is chosen as 200 $W/m^2/K$, sweep flow is 1.072 $mol.h^{-1}$ steam, channel pressures are 1 bar.

4.1.4. Investigation of Other Parameters

Figure 4.8 illustrates the relationship between CO conversion and channel pressures. The findings indicate that raising the channel pressure to 10 bar enhances CO conversion, reaching 98% for the ZIF-7 membrane and 95% for the Pd-Ag membrane. Additionally, CO conversion in the Pd-Ag membrane model appears to displays greater sensitivity to pressure increments.

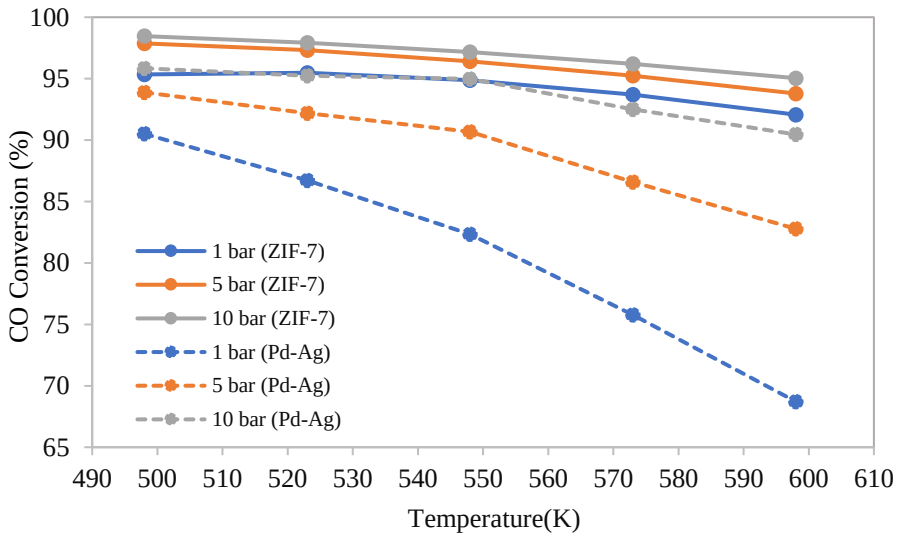

Figure 4.8. Effect of channel pressure on CO conversion, given pressures are valid for both channels.

The overall increase in conversions can be attributed to the rise in partial pressures of individual gases within both channels when pressure is set to a higher value. This leads to enhanced mass transfer through the membrane, resulting in higher CO conversion since the driving force for permeation is the difference in component partial pressures between the channels. Furthermore, there exists a maximum CO conversion limit under 100% in ZIF-7 membrane due to CO loss to the permeate channel, which also escalates with increasing pressure. Consequently, incremental pressure changes have a lesser impact on CO conversion in the ZIF-7 membrane compared to the Pd-Ag membrane.

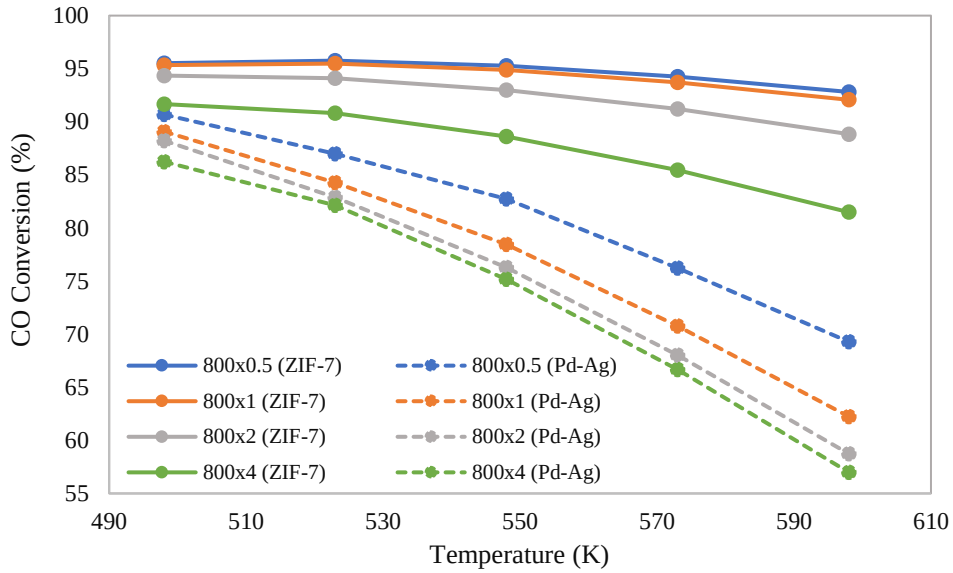

Figure 4.9. GHSV effect on CO conversion.

The impact of various inlet GHSV values on CO conversion can be examined using data from Figure 4.9. The figure shows that CO conversion peaks at 400 mol.h^{-1} for both membranes and declines with higher GHSV values. This trend occurs because altering the GHSV value directly affects the inlet molar flow rate of CO and consequently changes the residence time ($W/F_{co,in}$) of the gas mixture within the reactor. Decreasing the GHSV extends the residence time and consequently allows each gas component more time to pass through the membrane, resulting in higher CO conversion values.

Additionally, Pd-Ag membrane model displays a higher sensitivity to changes in GHSV, akin to its response to pressure variation. Conversely, decreasing GHSV levels provides minimal benefits for CO conversion on the ZIF-7 membrane model. This reduced impact of GHSV changes can be primarily attributed to CO loss present in ZIF-7 membrane model. Conversely, Pd-Ag membrane model is significantly impacted by GHSV alterations since it exhibits infinite selectivity to H_2 and lower H_2 permeability.

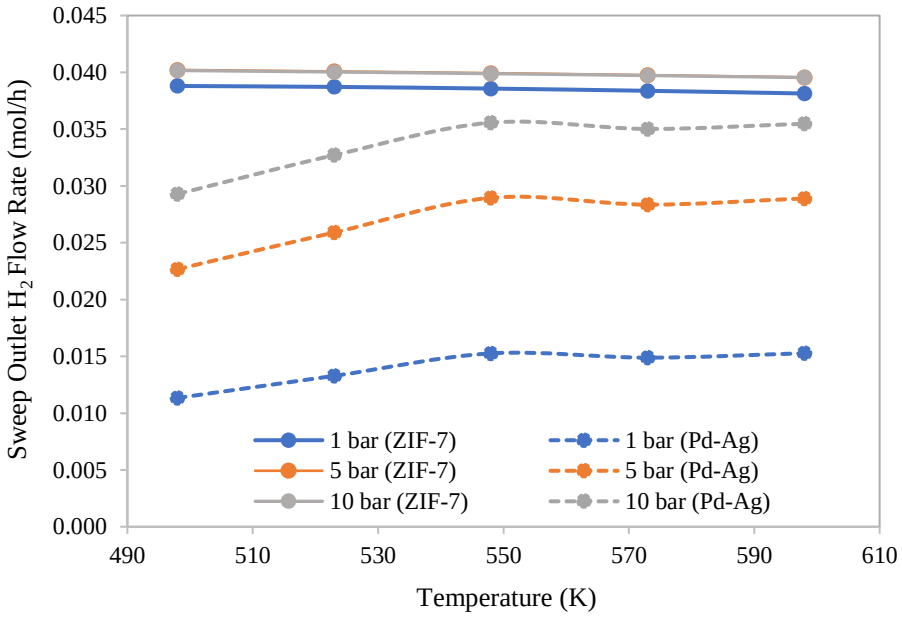

Figure 4.10. Effect of pressure on H_2 separation, 800h^{-1}, 1.072 mol.h^{-1} inlet sweep flowrate.

Figure 4.10 depicts the permeated H_2 flow rate at the outlet of the permeate channel across various pressure and temperature conditions. Here, it should be noted that the sum of the inlet molar flow rates of H_2 and CO amounts to 0.0428 mol.h^{-1}, indicating that 0.0428 mol.h^{-1} represents the maximum theoretical H_2 outlet flow rate in the permeate channel under conditions of 100% CO conversion and H_2 separation, with the assumption that there is no CO loss to the permeate channel. In ZIF-7 membrane model, the maximum H_2 sweep flow rate reaches 0.040 mol.h^{-1} and remains constant even after increasing pressure beyond 5 bar, as indicated in Figure 4.10. This phenomenon occurs due to a slight reverse permeation of gas components towards the outlet, leading to a partial pressure equilibrium state for all components. With increasing pressure, after a certain point within the reactor, the partial pressures at the retentate channel decrease further than those at the permeate channel primarily due to the high rate of H_2O reverse permeation and component loss to the permeate channel. Subsequently, H_2 partial pressure reaches equilibrium as reaction rates approach zero due to reaction equilibrium.

Moreover, given the lower H_2 permeance in the Pd-Ag membrane and its lower CO conversion rate, there is a reduced production and passage of H_2 through the membrane. Consequently, this leads to a lower H_2 retentate molar flow rate. Because of these given reasons and higher conversion resulted due to the transfer of H_2O through the membrane, partial pressure difference between the retentate and permeate channels approaches zero more rapidly in ZIF-7 membrane compared to the Pd-Ag membrane. Therefore, increasing the total pressure has a significantly greater effect on the Pd-Ag configuration.

The impact of temperature on the sweep H_2 molar flow rate is also minimal, as observed in Figure 4.10. At this point, it is important to remember that the permeance of H_2 only undergoes slight changes in response to temperature variations. Additionally, a larger portion of H_2 transfer occurs towards the reactor inlet, where the partial pressure difference is high, and this phenomenon is primarily dictated by the transfer through the membrane rather than the reaction due to the permeance of H_2 in ZIF-7 being larger compared to its permeance in Pd-Ag. Due to its lower H_2 permeance value and greater temperature dependence, the H_2 permeate flow rate in the Pd-Ag membrane model is relatively more susceptible to a variation in temperature.

4.2. WGS Modelling on Pt-CeO_2 Catalyst

4.2.1. Validation of the Non- membrane Model

CO conversion values are illustrated for both studies in the absence of a membrane in Figure 4.11. Our model results closely align with the CO conversion results given in Bac et al. [16] for both the model and experimental data. When the residence time is 23.7 g_{cat}.h/mol and in the temperature range of 200-275°C, it is evident that reaction rate is slow and equilibrium conditions are not present in the outlet of the reactor. However, as temperature rises, equilibrium conditions are met within the reactor due to faster reaction rates. Additionally, due to the exothermic nature of the WGS reaction, equilibrium conversion limit starts to get lower due to the Le Chatelier principle opposing the forward reaction as temperature increases. Therefore, equilibrium conditions are met easier within the reactor.

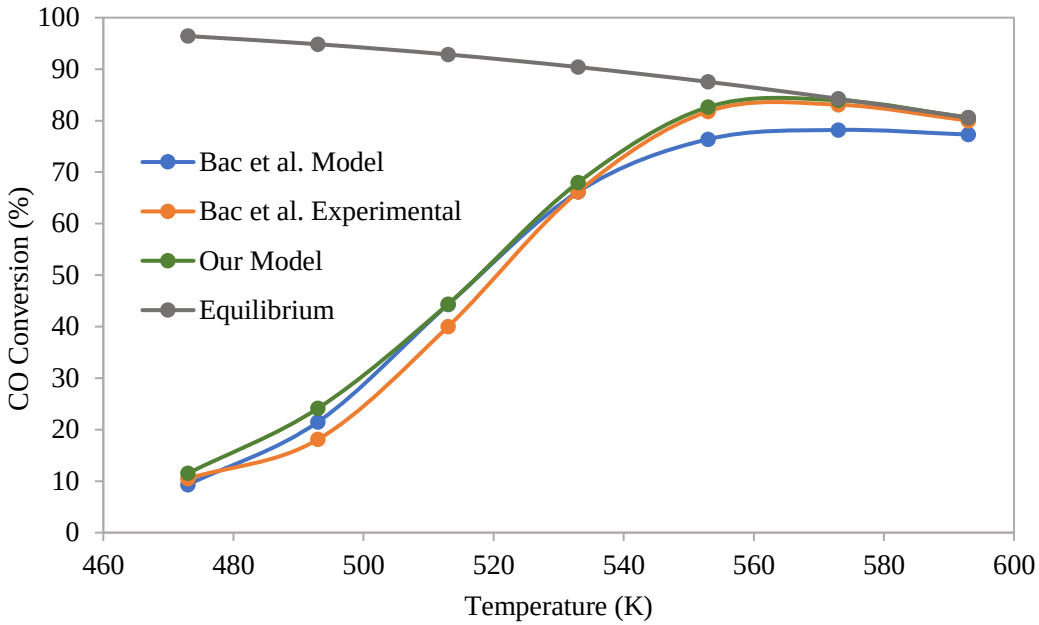

Figure 4.11. Equilibrium curve and conversion predictions of the model in this study and Bac et al. [16] for membraneless isothermal simulation at 1 bar.

4.2.2. Effect of Sweep Gas Type and Its Flowrate

Figure 4.12 illustrates the CO conversion data when employing either steam or argon as the sweep gas in a system where both permeate and retentate channels are kept constant at 1 bar, and the inlet molar flow rate of the retentate channel is set to the ten times of the parameter value used in the validation simulation, of which the results are previously illustrated in Figure 4.11, to model the reaction at higher pressures more accurately and to investigate the effect of the membrane at lower residence time values.

The minor elevation in CO conversion that can be observed in Figure 4.12 when argon is used as the sweep gas can be attributed to the transfer of H_2 through the ZIF-7 membrane. H_2 possesses the highest permeance value among the component gases and constitutes the highest fraction in the inlet. Consequently, its transfer through the membrane drives the reaction forward in accordance with the Le Chatélier Principle and results in higher CO conversion compared to the non-membrane case.

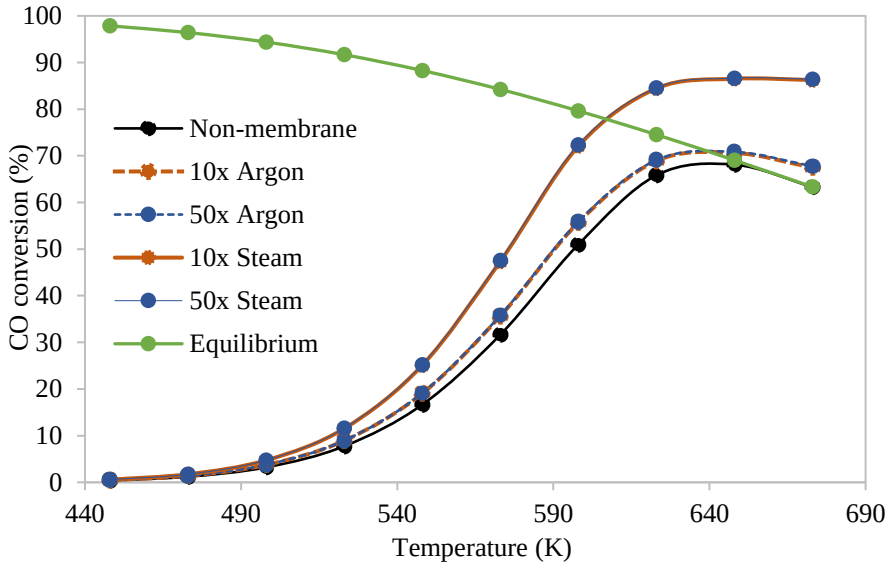

Figure 4.12. Effect of sweep type and molar flowrate (Residence time: 2.37 g_{cat}.h/mol, Retentate inlet molar flowrate (RIMF): 9.1x10^{-3} mol/h, 10-50x: 10-50 times of RIMF).

When compared to the improvement observed in Figure 4.4 and 4.5, however, CO conversion increment when Argon is used as the sweep gas seems relatively minor. CO conversion improvement that comes from using steam as the sweep gas is also slightly lesser. The notable difference in residence time between the two studies, with the model used to acquire the data in Figure 4.4 and 4.5 having a value of approximately 400 g.h/mol, is the primary reason for this outcome. This significantly larger residence time ensured that equilibrium conditions was attained at every temperature in the membraneless model and these conditions were present throughout a significant portion of the reactor, particularly at higher temperatures. However, reactor design in this model was initially optimized for the reaction to reach the equilibrium conditions nearly at the outlet in a membraneless model employed in Bac et al. Consequently, in this current membrane model, utilizing the membrane in the section that corresponds to the equilibrium portion in the membraneless model is not applicable. With increased residence time values, CO conversion can reach levels of 75-80% (as shown in Figure 4.13) for this setup, primarily due to the augmented membrane area when reactor diameter and bed density are held constant.

Figure 4.12 also reveals that employing steam as the sweep gas leads to a greater increase in CO conversion compared to using Argon. This can be easily attributed to the reverse-permeation of steam from the permeate channel to the retentate channel, which consequently elevates the partial pressure of steam in the retentate channel, thus driving the reaction forward according to Le Chatelier's Principle. By this way, increase in CO conversion can be achieved without the need to extend the residence time as previously discussed. Moreover, it can be seen in Figure 4.12 using a sweep gas flow rate equivalent to 10 times the molar flow rate at the retentate channel's inlet is sufficient to prevent excessive increase in component partial pressures in the permeate channel, thereby enabling the continued transfer through the membrane until the outlet of the reactor. Consequently, the 10xSteam sweep flow arrangement is adopted as the default for the remainder of the study.

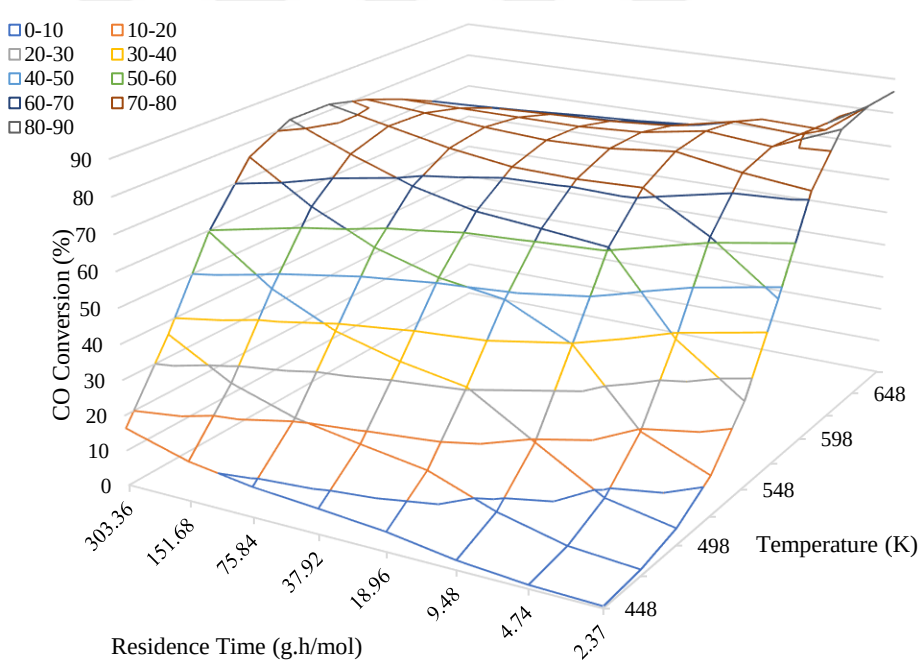

Figure 4.13. Residence time effect on CO conversion, sweep is 10x Argon, 1 bar.

4.2.3. Channel Pressure Effect

Figure 4.14 illustrates how CO conversion is influenced by the pressure within both channels in the membrane model. Also, given the black curve in Figure 4.14, it compares these resultant data with the data obtained from the non-membrane model under identical circumstances regarding the flow arrangement, inlet flow rate and reactor design. It is crucial to highlight that in the membrane models, both channels are maintained at the same pressure. Additionally, the decision to include the non-membrane model's 5-bar curve in Figure 4.14 for comparison stems from the fact that operation at 5 bar yields the highest CO conversion values in the non-membrane model.

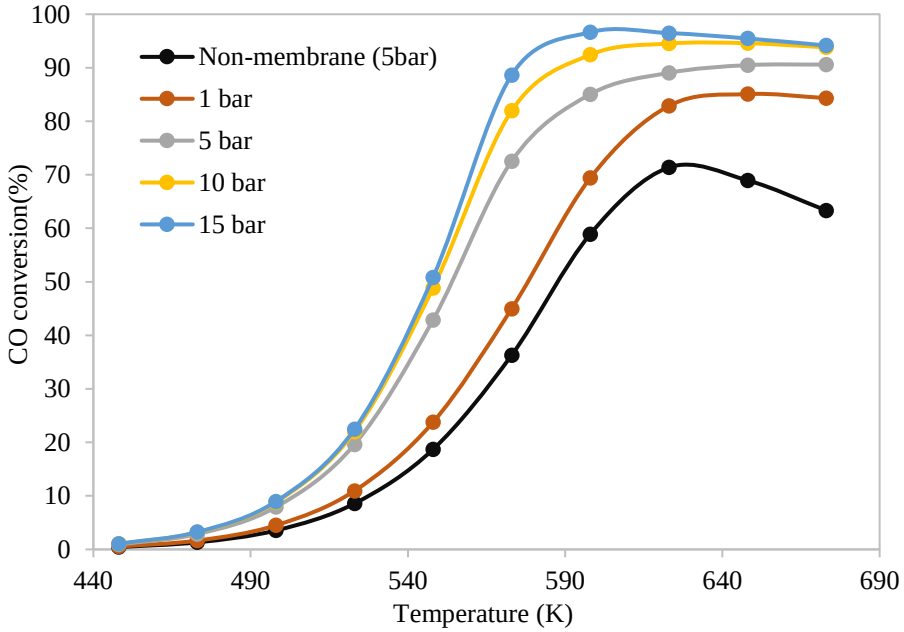

Figure 4.14. Effect of pressure on conversion, sweep gas is 10x Steam.

In Figure 4.14, the peak CO conversion rate, reaching approximately 97% at 325°C, is observed in the 15-bar curve, and CO conversion shows an increasing trend as operating pressure of the channels rises. These results are logical since higher pressure amplifies the partial pressure differences between the channels, thereby augmenting the transfer rates through the membrane and consequently increasing CO conversion. However, elevating the pressure beyond 10 bars in both channels does not appear to notably impact CO conversion.

The maximum increment in CO conversion, shifting from 10 bar to 15 bar, is less than 7% at 300°C and below 1% at 375 and 400°C. Consequently, a default setting of 10 bar pressure for both channels is adopted for further studies.

4.2.4. Effect of Sweep Gas Steam Flowrate at 10 bars

After selecting the 10-bar operation and steam as the sweep gas, effective molar flow rate of sweep gas is re-analyzed to account for a possible effect of pressure increase from 1 bar to 10 bar on CO conversion. Figure 4.15 illustrates the data acquired as a result of this investigation. Compared to Figure 4.5 and 4.12 where the pressure was 1 bar, data illustrated in Figure 4.15 is shows an interesting and contradicting behavior in the sense that increasing the steam flow rate at the inlet of the permeate channel result in a decrease in conversion at higher temperatures but in an increase at lower temperatures. Further investigation performed on the molar flow rates of the individual gas components within the reactor yielded an interesting reason for this phenomenon.

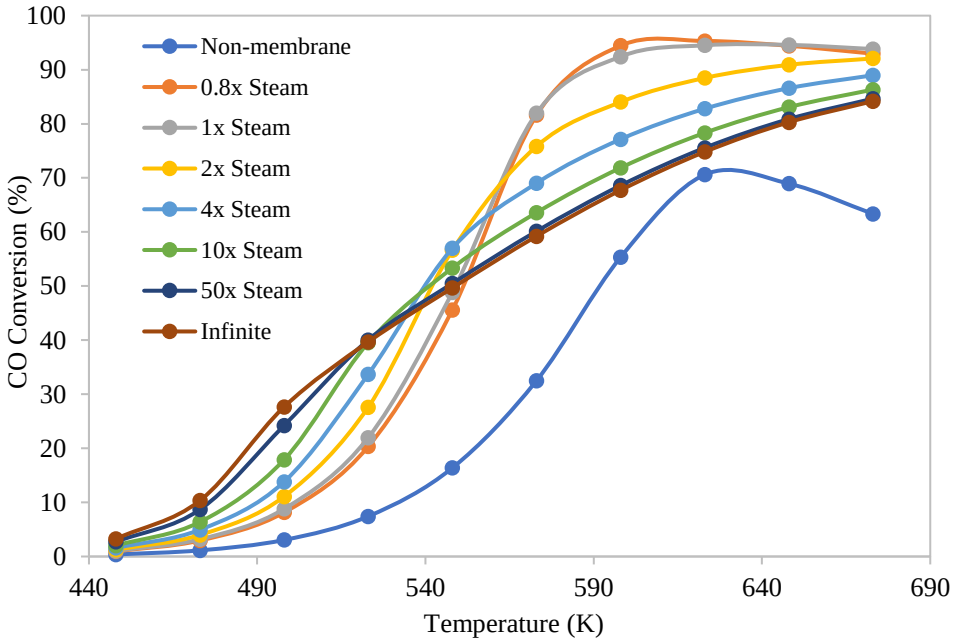

Figure 4.15. Effect of steam as sweep gas on conversion, 10 bar.

When sweep gas steam's molar flow rate is relatively low, its permeation from permeate to retentate channel leads to a faster partial pressure decrease in the permeate channel. When this rate of decrease is fast enough due to increased permeance of steam at higher temperatures, low enough molar flow rates and high membrane area per catalyst weight due the very small diameters of microreactors, partial pressures of other gases at permeate channel can get significantly higher than the partial pressures at the retentate side since their partial pressure at permeate channel is mostly affected by the transfer of another bulk gas rather than their own transfer through the membrane. Since partial pressure difference is the only driving force for the transfer through the membrane, permeation of CO, CO_2 and H_2 through the membrane starts to occur in reverse direction and this back-permeation is not immediately fast enough to counter the partial pressure increase of CO, CO_2 and H_2 within the permeate channel due to the transfer of steam. Important thing here is to note that back-permeation phenomenon is directly related to the fraction of the gases in the channels so amount of gas passed through the membrane becomes less-important if there is another mechanism that determines the fraction of gas components in the channels. That means, amount of CO passed through the membrane due to the partial pressure difference at the inlet can be a small proportion of the CO gas especially if its permeance is low. Thus, given that the residence time in the reactor is high enough to allow the back permeation of the CO gas and react within the retentate channel, CO loss is significantly mitigated and much of the CO manages enter the reaction due to the excess amount of steam present, resulting in the high CO conversion results at this small sweep gas flowrates.

However, the effect discussed above is also valid for both H_2 and CO_2 as well. Since these gases also back-permeate, the argument about disrupting the equilibrium and driving the reaction forward due to H_2 and CO_2 transfer through the membrane become less effective. Therefore, CO conversion depends on whether the effect of steam transfer and CO loss prevention or effect of H_2 and CO_2 permeation is stronger. It can be gleaned from Figure 4.12 that the former group is probably stronger than the H_2 and CO_2 removal in the reactor since conversion is noticeably improved when steam is used as the sweep gas and using Argon as the sweep gas improves the CO conversion very minimally compared to the non-membrane case. Additionally, partial pressure difference, mole fraction and amount of steam are quite high towards the permeate channel inlet compared to other gases at retentate.

Therefore, both the amount of steam and fraction, thus partial pressure of steam within the retentate channel is quite high compared to the other gases. Therefore, this high steam partial pressure will sufficiently drive the reaction forward until approximately 90% of CO conversion is achieved within the reactor.

The reason for the expected behavior of the curves at lower temperatures is the relatively lower permeance of steam in this temperature ranges and slower reaction rates. In these conditions, CO is consumed at a slower rate so its partial pressure also decreases slower and the amount lost to the permeate channel is higher. Additionally, due to its lower permeance value, steam within the permeate channel loses its partial pressure slower. As a result, back permeation starts to occur only towards the outlet of the reactor or is not even occur. This leads to a situation that is first described in section 4.1 in the reactor thus increasing sweep gas flow rate and driving the reaction as much as possible through removal of H_2 and supply of steam from permeate channel becomes more important in terms of achieving higher CO conversion.

However, despite the higher conversion values at higher temperatures, steam flow rate is kept at 10 times of RIMF for the following studies due to several reasons. The explanation given above is valid for the current model but since transfer occurring from retentate to permeate channel becomes non-existent at lower sweep gas molar flow rate applications towards the outlet due to the back permeation phenomenon, permeate channel flow also becomes non-existent especially at higher residence time (W/F_{co}) applications which is both unrealistic and problematic in terms of modelling. As the flow rate approaches zero, both denominator and nominator start to approach zero in partial pressure calculations and this still results in a relatively high partial pressure calculation due to the constant pressure assumption. In reality, however, this limit corresponds to a vacuum condition where partial pressure of each gas equates to zero. So, this discrepancy causes an uncertainty in the results when a lower sweep gas flow rate is utilized. Additionally, having high steam flow rate reduces the concentration of CO in the outlet stream and prevents a possible downstream process become poisoned. Therefore, selection of a higher steam flow rate is highly motivated.

4.2.5. Effect of Residence Time

Figure 4.16 illustrates the CO conversion results when residence time is varied between 2.37 to 35.55 g.h/mol. The results illustrated in the figure is expected since increasing residence time provides more catalyst weight and membrane area for reaction and transfer process to occur. One other important thing to notice that when residence time increased, conversion approaches 100% contrary to the results presented in Figure 4.9 where reducing GHSV values approaches to a limit conversion under 100%. This means that due to the usage of Pt-CeO_2 catalyst in the current inlet conditions, equilibrium conditions where each component's partial pressure in both channel is equal is not achieved contrary to Cu/Zn based catalyst case and initially lost CO is able to back-permeate and enter the reaction due to the transfer of steam from permeate to retentate channel reducing the partial pressure of CO in permeate channel.

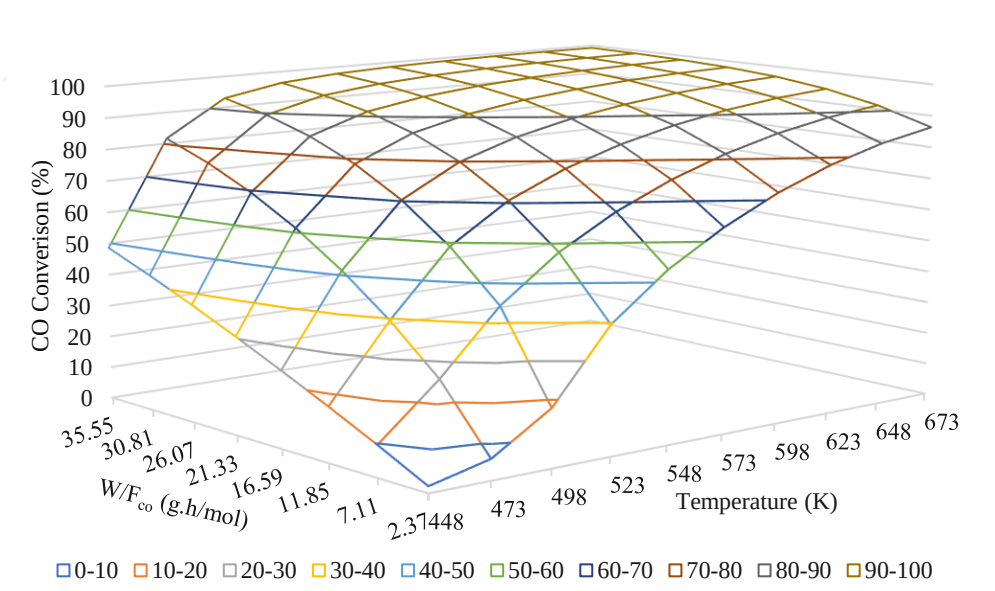

Figure 4.16. Effect of residence time on conversion, 10 bar, sweep gas:10xSteam.

4.2.6. Comparison with Conventional Process Mode

The results gathered from our model is also compared with the results gathered from employing the conventional two consecutive adiabatic membraneless reactor setup. Table 4.1 shows the results that are gathered from the model for the initial high temperature WGS reactor that operates under Fe/Cr based catalyst. Residence time column specifies the approximate residence time value that conversion just reaches its equilibrium value.

Table 4.1. Outlet data for the initial high temperature WGS reactor.

Inlet Temperature (°C)	Outlet Temperature (°C)	CO conversion (%)	W/F_{co} (g.h/mol)
350	445	52.66	18.963
375	462	48.59	9.956
400	479	44.53	5.926
425	497	40.48	3.319
450	514	36.43	1.778

Since equilibrium conversion decreases and reaction gets faster when temperature gets higher, both ultimate CO conversion value and necessary residence time to achieve it decreases. As residence time decreases, temperature difference between inlet and outlet also decreases since less time is spent for the exothermic reaction in the microreactor. Consequently, having an average temperature lower than 400°C and the highest ultimate conversion, the operation presented in the first row in Table 4.1 is selected as the upstream operation to the consecutive low temperature WGS reactor.

Inlet temperature is selected as 200°C and 250°C for the investigation of the next low temperature WGS reactor that operates under Cu/Zn based catalyst. CO conversion, residence time and outlet temperature data regarding these operations are presented in Table 4.2. In Table 4.2, total conversion equates to the total CO conversion that is achieved by using previously selected high temperature WGS reaction with the row of operation given in Table 4.2.

Table 4.2. Outlet data for the consecutive low temperature WGS reactor.

Inlet Temperature (°C)	Outlet Temperature (°C)	Single unit CO conversion (%)	Total Conversion(%)	W/F_{co} (g.h/mol)
200	268	76.93	89.08	1.20
250	306	63.97	82.94	0.45

As expected, 200°C operation results with a higher CO conversion but requires an higher residence time value to achieve it. However, compared to the former high temperature reaction, low temperature reaction requires much less catalyst weight and residence time value. Therefore, having a higher total conversion value, 200°C operation is selected as the default operation to be compared with the membrane reactor data. For this specific run, outlet CO and H_2 fractions are found as 1% and 19%, respectively.

Table 4.3. Outlet data for WGS membrane reactor. (Constant residence time).

Temperature (°C)	W/F_{co} (g.h/mol)	CO Conversion (%)	Retentate CO flow rate (mol/h^{-1})	Permeate CO flow rate (mol/h^{-1})	Retentate H_2 flow rate (mol/h^{-1})	Permeate H_2 flow rate (mol/h^{-1})
350	2.37	78.33	1.72E-06	1.96E-04	4.76E-04	2.97E-03
375	2.37	83.08	2.10E-06	1.52E-04	5.00E-04	2.99E-03
400	2.37	86.33	2.60E-06	1.22E-04	5.25E-04	3.00E-03

Table 4.3 presents the outlet data of the membrane reactor under Pt-CeO2 catalyst and previously selected default conditions. Looking at the Table 4.3, 400°C gives the highest conversion with 86% among these three runs. Also, 400°C operation has the lowest value for amount of CO lost the permeate channel and highest value for amount of H_2 produced. Additionally, the amount of CO present at the outlet of retentate channel is the highest for 400°C, hinting that further conversion is possible if the residence time is increased. Because of these reasons, 400°C operation seems better compared to the other two operations. Further investigation is also performed to analyze the results when residence time of the operation is increased. Table 4.4 presents the data regarding this investigation.

Table 4.4. Outlet data for WGS membrane reactor. (Constant Temperature).

Temperature (°C)	W/F_{co} (g.h/mol)	CO Conversion (%)	Retentate CO flow rate (mol/h^{-1})	Permeate CO flow rate (mol/h^{-1})	Retentate H_2 flow rate (mol/h^{-1})	Permeate H_2 flow rate (mol/h^{-1})
400	2.37	86.33	2.60E-06	1.22E-04	5.25E-04	3.00E-03
400	3.56	87.72	2.02E-06	1.10E-04	6.16E-04	2.92E-03
400	4.74	89.00	1.76E-06	9.85E-05	6.99E-04	2.85E-03
400	9.48	93.07	1.65E-06	6.15E-05	9.61E-04	2.62E-03
400	11.85	94.54	1.75E-06	4.80E-05	1.07E-03	2.53E-03

Based on the Table 4.4, 89% conversion can be acquired with 4.74 g.h/mol residence time operation and conversion can be further increased to 94% with 11.85 g.h/mol residence time operation. Also, total amount of H_2 produced also slightly increases as residence time gets larger. However, H_2 recovery in permeate channel also gets poorer with increasing residence time due to its back permeation and nonnegligible amount of H_2 is still present in the retentate channel for most of the case. Therefore, at this point, optimum result might be different depending on the application and parameters such as CO conversion, catalyst weight (residence time), total or separated H_2 flow, normal or dry (without H_2O) mole fraction of CO and H_2 at the channel outlets or in mixed conditions are the deciding factors for the optimal decision. Table 4.5 presents these data for the residence time cases with 2.37 (Process 1), 4.74 (Process 2), 11.85 (Process 3) g.h/mol and conventional two consecutive reactor operation.

Table 4.5. Comparison between the selected processes.

	Process 1	Process 2	Process 3	Conventional Operation
CO Conversion (%)	86.33	89.00	94.54	89.08
W/F_{co} (g.h/mol)	2.37	4.74	11.85	Fe/Cr: 18.96 Cu/Zn: 1.20
Total H_2 flow rate (mol/h^{-1})	3.52E-03	3.54E-03	3.60E-03	3.55E-03

Table 4.5. Comparison between the selected processes. (cont.)

	Process 1	Process 2	Process 3	Conventional Operation
Permeate H_2 flow rate (mol/h^{-1})	3.00E-03	2.85E-03	2.53E-03	N/A
Permeate CO mol fraction	1.44E-03	1.24E-03	6.90E-04	N/A
Permeate H_2 mol fraction	3.55E-02	3.58E-02	3.63E-02	N/A
Total CO mol fraction	1.24E-03	1.00E-03	4.97E-04	1.09E-02
Total H_2 mol fraction	3.51E-02	3.54E-02	3.59E-02	3.89E-01
Permeate CO dry mol fraction	2.95E-02	2.36E-02	1.25E-02	N/A
Permeate H_2 dry mol fraction	7.25E-01	6.81E-01	6.57E-01	N/A
Total CO dry mol fraction	1.53E-02	1.23E-02	6.11E-03	1.23E-02
Total H_2 dry mol fraction	4.32E-01	4.35E-01	4.41E-01	4.38E-01

In terms of outlet H_2 flow rate, unless the outlet flows of individual channels are mixed in membrane models, permeate channel H_2 flowrates are lower than the outlet flow rate of the conventional process. In a situation where the outlet flows are mixed, however, process 3 offers the highest H_2 flow rate by a slight margin among these four processes.

Mixing the outlet of the two flow also increases the CO content of the flow that goes to the downstream processes. Usually, these processes involve further separation units that reduces the CO concentration to ppm levels. Therefore, outlet flow having a lower CO concentration is crucial in terms of relaxing the conditions on these downstream processes. Thus, optimal decision about mixing the two channel outlets depends on the target H_2 production and possible relaxation on the downstream separation processes.

Looking at the CO and H_2 fractions presented in Table 4.5 for the membrane processes, process 3 has the highest H_2 fraction and the lowest CO fraction due to the higher conversion as expected. Compared to the conventional process, all these three processes have lower CO and H_2 fractions since steam that permeates from permeate to retentate channel significantly decreases the fractions of these gases. Consequently, comparing the dry fractions, (amount of steam is excluded) of each process is more reliable since one of the main goal is also having H_2 as pure as possible and separating steam from the other components is also relatively easy.

Considering the dry fractions, process 3 is better compared to the other three processes in terms of having lower CO dry fraction on the permeate channel and in mixed conditions (0.62 % lower CO dry fraction compared to the conventional process). It has also slightly the highest total H_2 dry fraction compared to the other processes. However, due to the presence of back permeation, it's permeate dry H_2 fraction is lower than the process 1 and 2.

From the overall results presented above, process 3 seems to have better results compared to the other three processes. However, optimum decision heavily depends on required residence time to achieve the results given in Table 4.5. Overall, membrane processes require catalyst weight lower than the conventional processes but the difference is significantly higher between the process 1 and 4. If CO fraction is less important, process 1 might as well be the optimum choice since total H_2 molar flow rates and total H_2 dry fractions are relatively close to each other for all four processes. Additionally, conventional process requires cooling from 445°C to 200°C between the two reactors to achieve the results in Table 4.5, whereas process 1 to 3 requires heating from 350°C to 400°C prior to the membrane reactor assuming the upstream is 350°C. As a result, it can be concluded that ZIF-7 membrane reactor is able to offer better performance compared to the conventional process in terms of CO conversion and H_2 production.

5. CONCLUSION

The developed relatively simple 1D isothermal steady state mathematical models investigate WGS reaction occurring on Cu/Zn and Pt-CeO_2 catalyst in a ZIF-7 membrane. Parameters regarding the ZIF-7 Membrane are taken from the work of Lee et al. and employed in both models. In the model with Cu/Zn catalyst, reactor conditions are set to reflect the conditions presented in the work of Lee et al. and model results are validated with the experimental data given in the said work. The model is then used to analyze the effects of sweep flow type, rate and arrangement and 1.072 $mol.h^{-1}$ $H_2O_{(g)}$ in co-current flow is found to be suitable for ZIF-7 membrane with current specific set of inlet conditions and reactor geometry both in terms of resulting in higher CO conversion and ensuring an isothermal operation. Further studies involving the GHSV and pressure of the channels has shown that 10 bar operation with $800h^{-1}$ GHSV is important to keep the outlet flow rates high while maintaining a maximized CO conversion value. Additionally, parametric studies also managed to show the advantage of using ZIF-7 membrane over the Pd-Ag membrane in terms of CO conversion and H_2 flow rate at permeate channel outlet.

In the model with Pt-CeO_2 catalyst, reactor conditions and geometry are set to the conditions presented in the Bac et al. Similar to the previous model, non-membrane results gathered from our model are validated via the method of comparison with the results given in the said work. Effect of sweep gas type and flow rate is also investigated in a co-current arrangement at 1 bar and using steam at 10 times of the RIMF ($9.11x10^{-2}$ $mol.h^{-1}$ steam flow) as the sweep gas is found to be the most efficient to get a reasonably high 86.7% CO conversion maximum at 648 K.

Following pressure study resulted in the selection of 10 bars operation since higher pressures did not increase the CO conversion significantly and investigation of sweep gas flowrate is repeated at 10 bars pressure. It is found that back permeation of the species caused a drop on CO conversion as sweep gas flowrate is set to a larger value above 573 K.

However, it is also shown that the reliability of the results starts to decline as temperature and flowrate of the sweep gas simultaneously increase and decrease, respectively. Because of that, previously selected $9.11x10^{-2}$ $mol.h^{-1}$ steam flow kept as the default flow for the permeate channel. Following residence times investigation shown that the CO conversion manages to approach 100% conversion as residence time and temperature approaches 35.55 g.h/mol and 673 K, respectively.

Lastly, conventional two consecutive adiabatic reactor operation is modeled and the results are compared to the current model. Upstream is assumed to be 350°C and optimal conditions for the first high temperature reactor in conventional process in terms of CO conversion and temperature are found to be 350°C inlet with 18.963 g.h/mol residence time at 10 bar pressure. For the second low temperature reactor, 200°C inlet with 1.20 g.h/mol residence time is found to be the most optimal and ultimate CO conversion at the end of this two-reactor configuration is found to be 89.08%. Residence time and temperature investigation for membrane microreactor concluded with the three optimal processes that can be compared with the conventional reactor (Table 4.5). Membrane reactor with 11.85 g.h/mol residence time at 400°C is found to be the most optimal in terms of CO conversion, outlet H_2 flow rate, H_2 dry fraction and CO dry fraction. However, lower residence time membrane microreactor processes (Process 1 and 2) can also be preferable due to their lower residence time requirement. Nevertheless, it is shown that microreactor membrane processes with Pt-CeO_2 catalyst are superior compared to the conventional reactor in that close or even better outcomes can be acquired with less residence time, heat duty and availability of isothermal conditions.

REFERENCES

1. Chen, W.-H., J. Peng, and X. T. Bi, “A State-of-the-Art Review of Biomass Torrefaction, Densification and Applications”, *Renewable and Sustainable Energy Reviews*, Vol. 44, pp. 847–866, 2015.

2. International Energy Agency, “World Energy Outlook 2023”, 2023, https://www.iea.org/reports/world-energy-outlook-2023, accessed on June 29, 2024.

3. Chen, W.-H., and C.-Y. Chen, “Water Gas Shift Reaction for Hydrogen Production and Carbon Dioxide Capture: A Review”, *Applied Energy*, Vol. 258, pp. 114078-114079, 2020.

4. Wu, C., Q. Huang, Z. Xu, A. T. Sipra, N. Gao, L. P. S Vandenberghe, S. Vieira, C. R. Soccol, R. Zhao, S. Deng, S. K. S. Boetcher, S. Lu, H. Shi, D. Zhao, Y. Xing, Y. Chen, J. Zhu, D. Fen, Y. Zhan, L. Deng, G. Hu, P. A. Webley, D. Liang, Z. Ba, A. M-Medrala, A. Magdziarz, N. Miskolczi, S. Tomasek, S. S Lam, S. Y. Foong, H. S. Ng, L. Jiang, X. Yan, Y. Liu, Y. Ji, H. Sun, Y. Zhang, H. Yang, X. Zhang, M. Sun, D. C.W. Tsang, J. Shang, C. Muller, M. Rekhtina, M. Krodel, A. H. Bork, F. Donat, L. Liu, X. Jin, W. Liu, S. Saqline, X. Wu, Y. Xu, A. L. Khan, Z. Ali, H. Lin, L. Hu., J. Huang, R. Singh, K. Wang, X. He, Z. Dai, S. Yi, A. Konist, M. H. S. Baqain, Y. Zhao, S. Sun, G. Chen, X. Tu, A. Weidenkaff, S. Kawi, K. H. Lim, C. Song, Q. Yang, Z. Zhao, X. Gao, X. Jiang, H. Ji, T. E. Akinola, A. Lawal, O. S. Otitoju, M. Wang, G. Zhang, L. Ma, B. C. Sempuga, X. Liu, E. Oko, M. Daramola, Z. Yu, S. Chen, G. Kang, Q. Li, L. Gao, L. Liu, and H. Zhou, “A Comprehensive Review of Carbon Capture Science and Technologies”, *Carbon Capture Science & Technology*, Vol. 11, pp. 100178 - 100179, 2024.

5. Saeidi, S., F. Fazlollahi, S. Najari, D. Iranshahi, J. J. Klemeš, and L. L. Baxter, “Hydrogen Production: Perspectives, Separation with Special Emphasis on Kinetics of WGS Reaction: A State-of-the-Art Review”, *Journal of Industrial and Engineering Chemistry*, Vol. 49, pp. 1–25, 2017.

6. Pal, D. B., R. Chand, S. N. Upadhyay, and P. K. Mishra, “Performance of Water Gas Shift Reaction Catalysts: A Review”, *Renewable and Sustainable Energy Reviews*, Vol. 93, pp. 549–565, 2018.

7. Kolb, G., “Review: Microstructured Reactors for Distributed and Renewable Production of Fuels and Electrical Energy”, *Chemical Engineering and Processing: Process Intensification*, Vol. 65, pp. 1–44, 2013.

8. Trimm, D.L., and Z. I. Önsan, “Onboard Fuel Conversion for Hydrogen-Fuel-Cell-Driven Vehicles”, *Catalysis Reviews*, Vol. 43, No. 1–2, pp. 31–84, 2001.

9. Zhu, M., and I. E. Wachs, “Iron-Based Catalysts for the High-Temperature Water–Gas Shift (HT-WGS) Reaction: A Review”, *ACS Catalysis*, Vol. 6, No. 2, pp. 722–732, 2016.

10. Zhang, H., Z. Sun, and Y. H. Hu, “Steam Reforming of Methane: Current States of Catalyst Design and Process Upgrading”, *Renewable and Sustainable Energy Reviews*, Vol. 149, pp. 111330-111331, 2021.

11. Ratnasamy, C., and J. P. Wagner, “Water Gas Shift Catalysis”, *Catalysis Reviews*, Vol. 51, No. 3, pp. 325–440, 2009.

12. Saeidi, S., A. Sapi, A. H. Khoja, S. Najari, M. Ayesha, Z. Kónya, B. B. Asare-Bediako, A. Tatarczuk, V. Hessel, F. J. Keil, and A. E. Rodrigues, “Evolution Paths from Gray to Turquoise Hydrogen via Catalytic Steam Methane Reforming: Current Challenges and Future Developments”, *Renewable and Sustainable Energy Reviews*, Vol. 183, pp. 113392 - 113393, 2023.

13. Luengnaruemitchai, A., S. Osuwan, and E. Gulari, “Comparative Studies of Low-Temperature Water–Gas Shift Reaction over Pt/CeO_2, Au/CeO_2, and Au/Fe_2O_3 Catalysts”, *Catalysis Communications*, Vol. 4, No. 5, pp. 215–221, 2003.

14. Yin, H., J. Shang, J. Choi, and A. C. K. Yip, “Generation and Extraction of Hydrogen from Low-Temperature Water-Gas-Shift Reaction by a ZIF-8-based Membrane Reactor”, *Microporous and Mesoporous Materials*, Vol. 280, pp. 347–356, 2019.

15. Kim, J. and D. Lee, “Marked Inducing Effects of Metal Oxide Supports on the Hydrothermal Stability of Zeolitic Imidazolate Framework (ZIF) Membranes”, *Journal of Materials Chemistry A*, Vol. 4, No. 14, pp. 5205–5215, 2016.

16. Bac, S., S. Keskin, and A. K. Avci, “Modeling and Simulation of Water-Gas Shift in a Heat Exchange Integrated Microchannel Converter”, *International Journal of Hydrogen Energy*, Vol. 43, No. 2, pp. 1094–1104, 2018.

17. Khan, A., P. Chen, P. Boolchand, and P. Smirniotis, “Modified Nano-Crystalline Ferrites for High-Temperature WGS Membrane Reactor Applications”, *Journal of Catalysis*, Vol. 253, No. 1, pp. 91–104, 2008.

18. Reddy, G. K., P. Boolchand, and P. G. Smirniotis, “Sulfur Tolerant Metal Doped Fe/Ce Catalysts for High Temperature WGS Reaction at Low Steam to CO Ratios – XPS and Mössbauer Spectroscopic Study”, *Journal of Catalysis*, Vol. 282, No. 2, pp. 258–269, 2011.

19. Devaiah, D., and P. G. Smirniotis, “Effects of the Ce and Cr Contents in Fe–Ce–Cr Ferrite Spinels on the High-Temperature Water–Gas Shift Reaction”, *Industrial & Engineering Chemistry Research*, Vol. 56, No. 7, pp. 1772–1781, 2017.

20. Kim, S.-J., Z. Xu, G. K. Reddy, P. Smirniotis, and J. Dong, “Effect of Pressure on High-Temperature Water Gas Shift Reaction in Microporous Zeolite Membrane Reactor”, *Industrial & Engineering Chemistry Research*, Vol. 51, No. 3, pp. 1364–1375, 2012.

21. Chen, W.-H., C.-W. Tsai, Y.-L. Lin, R.-Y. Chein, and C.-T. Yu, “Reaction Phenomena of High-Temperature Water Gas Shift Reaction in a Membrane Reactor”, *Fuel*, Vol. 199, pp. 358–371, 2017.

22. Panagiotopoulou, P., and D. I. Kondarides, “A Comparative Study of the Water-Gas Shift Activity of Pt Catalysts Supported on Single (MO_x) and Composite (MO_x/Al_2O_3, MO_x/TiO_2) Metal Oxide Carriers”, *Catalysis Today*, Vol. 127, No. 1–4, pp. 319–329, 2007.

23. Jeong, D.-W, H. S. Potdar, J.-O. Shim, W.-J. Jang, and H.-S. Roh, “H_2 Production from a Single Stage Water–Gas Shift Reaction over Pt/CeO_2, Pt/ZrO_2, and $Pt/Ce_{(1-x)}Zr_{(x)}O_2$ Catalysts”, *International Journal of Hydrogen Energy*, Vol. 38, No. 11, pp. 4502–4507, 2013.

24. Cornaglia, C. A., S. Tosti, M. Sansovini, J. Múnera, and E. A. Lombardo, “Novel Catalyst for the WGS Reaction in a Pd-Membrane Reactor”, *Applied Catalysis A: General*, Vol. 462–463, pp. 278–286, 2013.

25. Jeong, D.-W., W.-J. Jang, J.-O. Shim, W.-B. Han, K.-W. Jeon, Y.-C. Seo, H.-S. Roh, J.-H. Gu, and Y. T. Lim, “Low-Temperature Water–Gas Shift Reaction Over Supported Cu Catalysts”, *Renewable Energy*, Vol. 65, pp. 102–107, 2014.

26. Shim, J.-O., H.-S. Na, S.-Y. Ahn, K.-W. Jeon, W.-J. Jang, B.-H. Jeon, and H.-S. Roh, “An Important Parameter for Synthesis of Al_2O_3 Supported Cu-Zn Catalysts in Low-Temperature Water-Gas Shift Reaction Under Practical Reaction Condition”, *International Journal of Hydrogen Energy*, Vol. 44, No. 29, pp. 14853–14860, 2019.

27. Sagata, K., N. Imazu, and H. Yahiro, “Study on Factors Controlling Catalytic Activity for Low-Temperature Water–Gas-Shift Reaction on Cu-based Catalysts”, *Catalysis Today*, Vol. 201, pp. 145–150, 2013.

28. Li, Y., Q. Fu, and M. Flytzani-Stephanopoulos, “Low-Temperature Water-Gas Shift Reaction over Cu- and Ni-loaded Cerium Oxide Catalysts”, *Applied Catalysis B: Environmental*, Vol. 27, No. 3, pp. 179–191, 2000.

29. Mendes, D., V. A. Gomes, J. Zheng, S. Tosti, F. Borgognoni, A. Mendes, and L. M. Madeira, “Enhancing the Production of Hydrogen via Water–Gas Shift Reaction Using Pd-based Membrane Reactors”, *International Journal of Hydrogen Energy*, Vol. 35, No. 22, pp. 12596–12608, 2010.

30. Liguori, S., P. Pinacci, P. K. Seelam, R. Keiski, F. Drago, V. Calabrò, A. Basile, and A. Iulianelli, “Performance of a Pd/PSS Membrane Reactor to Produce High Purity Hydrogen via WGS Reaction”, *Catalysis Today*, Vol. 193, No. 1, pp. 87–94, 2012.

31. Brunetti, A., G. Barbieri, E. Drioli, T. Granato, and K.-H. Lee, “A Porous Stainless Steel Supported Silica Membrane for WGS Reaction in a Catalytic Membrane Reactor”, *Chemical Engineering Science*, Vol. 62, No. 18–20, pp. 5621–5626, 2007.

32. Araki, S., H. Miyanishi, H. Yano, S. Tanaka, and Y. Miyake, “Water Gas Shift Reaction in a Membrane Reactor Using a High Hydrogen Permselective Silica Membrane”, *Separation Science and Technology*, Vol. 48, No. 1, pp. 76–83, 2013.

33. Zhang, Y., Z. Wu, Z. Hong, X. Gu, and N. Xu, “Hydrogen-Selective Zeolite Membrane Reactor for Low Temperature Water Gas Shift Reaction”, *Chemical Engineering Journal*, Vol. 197, pp. 314–321, 2012.

34. Tang, Z., S.-J. Kim, G. K. Reddy, J. Dong, and P. Smirniotis, “Modified Zeolite Membrane Reactor for High Temperature Water Gas Shift Reaction”, *Journal of Membrane Science*, Vol. 354, No. 1–2, pp. 114–122, 2010.

35. Yin, H., J. Shang, J. Choi, and A. C. K. Yip, “Generation and Extraction of Hydrogen from Low-Temperature Water-Gas-Shift Reaction by a ZIF-8-based Membrane Reactor”, *Microporous and Mesoporous Materials*, Vol. 280, pp. 347–356, 2019.

36. Li, Y., F. Liang, H. Bux, W. Yang, and J. Caro, “Zeolitic Imidazolate framework ZIF-7 Based Molecular Sieve Membrane for Hydrogen Separation”, *Journal of Membrane Science*, Vol. 354, No. 1–2, pp. 48–54, 2010.

37. Huang, A., Y. Chen, N. Wang, Z. Hu, J. Jiang, and J. Caro, “A Highly Permeable and Selective Zeolitic Imidazolate Framework ZIF-95 Membrane for H_2/CO_2 Separation”, *Chemical Communications*, Vol. 48, No. 89, pp. 10981-10983, 2012.

38. Amadeo, N., “Hydrogen Production from the Low-temperature Water-Gas Shift Reaction: Kinetics and Simulation of the Industrial reactor”, *International Journal of Hydrogen Energy*, Vol. 20, No. 12, pp. 949–956, 1995.

39. Moe, J. M. “Design of Water Gas Shift Reactors.”, *Chemical Engineering Progress*, Vol. 58, pp. 33–36, 1962.

40. Phatak, A. A., N. Koryabkina, S. Rai, J. L. Ratts, W. Ruettinger, R. J. Farrauto, G. E. Blau, W. N. Delgass, and F. H. Ribeiro, “Kinetics of the Water–Gas Shift Reaction on Pt Catalysts Supported on Alumina and Ceria”, *Catalysis Today*, Vol. 123, No. 1–4, pp. 224–234, 2007.

41. Hla, S., G. J. Duffy, J. H. Edwards, Daniel G. Roberts, Alexander Y. Ilyushechkin, L. D. Morpeth, and T. Nguyen “Kinetics of High-Temperature Water-Gas Shift Reaction over Two Iron-based Commercial Catalysts Using Simulated Coal-derived Syngases”, *Chemical Engineering Journal*, Vol. 146, No. 1, pp. 148–154, 2009.

42. Lee, S., J. Kim, J. Kim, and D. Lee, “Zeolitic Imidazolate Framework Membrane with Marked Thermochemical Stability for High-Temperature Catalytic Processes”, *Chemistry of Materials*, Vol. 30, No. 2, pp. 447–455, 2018.

43. Germani, G., and Y. Schuurman, “Water-Gas Shift Reaction Kinetics over μ-structured $Pt/CeO_2/Al_2O_3$ Catalysts”, *AIChE Journal*, Vol. 52, No. 5, pp. 1806–1813, 2006..

44. Kim, J., and D. Lee, “Marked Inducing Effects of Metal Oxide Supports on the Hydrothermal Stability of Zeolitic Imidazolate Framework (ZIF) Membranes”, *Journal of Materials Chemistry A*, Vol. 4, No. 14, pp. 5205–5215, 2016.

45. Germani, G., P. Alphonse, M. Courty, Y. Schuurman, and C. Mirodatos, “Platinum/ceria/alumina Catalysts on Microstructures for Carbon Monoxide Conversion”, *Catalysis Today*, Vol. 110, No. 1–2, pp. 114–120, Dec. 2005.

46. Choi, Y., and H. G. Stenger, “Water Gas Shift Reaction Kinetics and Reactor Modeling for Fuel Cell Grade Hydrogen”, *Journal of Power Sources*, Vol. 124, No. 2, pp. 432–439, 2003.

47. Bohlbro, H., N. C. Li, J. Yu, H. Dam, B. Sjöberg, and J. Toft, “The Kinetics of the Water Gas Conversion at Atmospheric Pressure.”, *Acta Chemica Scandinavica*, Vol. 15, pp. 502–520, 1961.

48. Bohlbro, H., B. Nilsson, C. Krohn, K. Motzfeldt, O. Theander, and H. Flood, “The Kinetics of the Water Gas Conversion. II. Investigations at Elevated Pressures.”, *Acta Chemica Scandinavica*, Vol. 16, pp. 431–438, 1962.